Inorganic Chemistry
Cite This: Inorg. Chem. 2018, 57, 7299−7313
Article
pubs.acs.org/IC

Influences of Cation Ratio, Anion Type, and Water Content on Polytypism of Layered Double Hydroxides

Meng Chen,*[,†,§] Runliang Zhu,[†,§] Xiancai Lu,[‡] Jianxi Zhu,[†,§] and Hongping He[†,§]

[†]CAS Key Laboratory of Mineralogy and Metallogeny/Guangdong Provincial Key Laboratory of Mineral Physics and Materials, Guangzhou Institute of Geochemistry, Chinese Academy of Sciences (CAS), Guangzhou 510640, China

[‡]State Key Laboratory for Mineral Deposits Research, School of Earth Sciences and Engineering, Nanjing University, Nanjing 210093, China

[§]University of Chinese Academy of Sciences, 19 Yuquan Road, Beijing 100049, China

Supporting Information

ABSTRACT: Layered double hydroxides (LDHs) are a significant sink of anions (CO_3^{2-}, SO_4^{2-}, NO_3^-, Cl^-, etc.) and divalent transition-metal cations in soil. The anion exchange capacity gives rise to functional materials. The stability of LDHs is determined by the interaction between cation-bearing layers and intercalated water and anions, which is correlated with polytypism and coordination structure. A systematic investigation is performed to show the influence of cation ratio, anion type, and water content on polytypism, swelling behavior, and interlayer structure of Mg−Al-LDHs using molecular dynamics simulations. LDHs intercalated with NO_3^- ions exhibit a polytype transition from $3R_1$ (three-layer rhombohedral polytype) to $1T$ (one-layer trigonal polytype) with increasing water content. NO_3^- ions exhibit a D_{3h} point group symmetry at low water contents. The polytype transition coincides with the complete transformation into tilted NO_3^- ion with a C_{2v} point group symmetry. The transition appears at a lower water content when the Mg/Al ratio is lower. LDHs with SO_4^{2-} ions exhibit a three-stage polytypism. The first and last stages are $3R_1$. The intermediate stage could be $1T$ or a mixture of different O(octahedra)-type interlayers, which depends on the cation ratio. The relative popularity of SO_4^{2-} ions with a C_s point group symmetry is characteristic for the intermediate stage, while mostly SO_4^{2-} ions exhibit a C_{3v} symmetry. There is no clear relevance between cation ratio and water content at which a polytype transition happens. The configurational adjustments of NO_3^- and SO_4^{2-} ions facilitate the swelling behavior of LDHs. LDHs with CO_3^{2-} or Cl^- ions always maintain a $3R_1$ polytype irrespective of water content and hardly swell. The configurations of anions and water reflect local coordination structure due to hydrogen bonds. The layer-stacking way influences long-ranged Coulombic interactions. Hydrogen-bonding structure and long-ranged Coulombic interactions collectively determine polytypism and stability of LDHs.

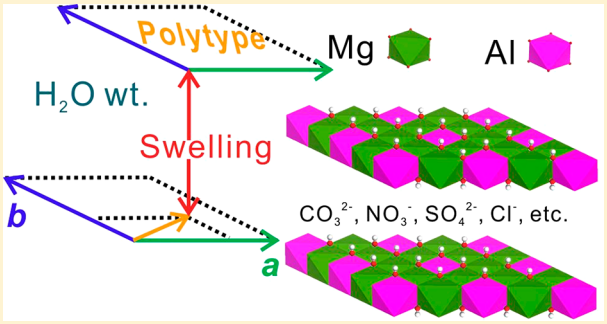

1. INTRODUCTION

Layered double hydroxides (LDHs), with the general chemical formula $[M^{II}_{1-x}M^{III}_x(OH)_2](A^{n-})_{x/n}\cdot mH_2O$, are a class of natural and synthetic inorganic compounds with layered structure derived from that of brucite $Mg(OH)_2$. Natural occurrences of LDHs are generally associated with serpentine and carbonate.[1−3] Although natural stocks of them are limited, they are commonly precipitated in contaminated soil, as a significant sink of transition-metal ions (Zn(II), Ni(II), Co(II), and Fe(II)) in the environment.[4−10] Divalent metal cations are adsorbed onto surfaces of clay minerals or gibbsite in soil, with dissolution of Al from minerals, which leads to nucleation and growth of mixed-metal(II)-Al LDHs.[11−19] Thermodynamic studies showed the formation of LDHs is favored over that of pure metal hydroxides.[20−23] Anions (A^{n-}) intercalated in LDHs can be CO_3^{2-}, SO_4^{2-}, NO_3^-, Cl^-, etc., which are exchangeable.[24] It was suggested anions are much more important than cations in determining the solubility of LDHs.[21] Calorimetric studies disclosed the thermodynamic stability of LDHs intercalated with different anions follows the order $NO_3^- < SO_4^{2} < CO_3^{2-}$,[21,25] consistent with the order of anion exchange capacity ($NO_3^- > Cl^- > SO_4^{2} > CO_3^{2-}$)[24] and that of the magnitude of the binding energy ($NO_3^- < Cl^- < SO_4^{2} < CO_3^{2-}$).[26] Based on thermodynamic data and measured concentrations of ions in soil, LDHs with CO_3^{2-} were shown to be more preferable than those with Cl^-.[7] A dissolution kinetics study showed, with a silicate-for-nitrate exchange in the interlayer, LDHs become much more stable.[16] These studies show the importance of anions in stability of LDHs.

Besides anions, intercalated water is also relevant to the structure and properties of LDHs. The behavior of it is intermediate between solid ice and liquid water.[20,27−30] Water molecules are fixed in sites of the interlayer like atoms in the

Received: April 10, 2018
Published: June 4, 2018

DOI: 10.1021/acs.inorgchem.8b00949
Inorg. Chem. 2018, 57, 7299−7313

solid lattice, and they diffuse through hopping between adjacent sites.[31,32] With moveable water and anions in the interlayer galleries, LDHs exhibit characteristics such as anion exchanges,[33−35] hydration,[36] dehydration,[37−39] and protonic conduction.[40] Such characteristics are relevant to their roles as catalysts, catalyst supports, adsorbing agents, electrode modifiers, and so on.[41−45] Organic compounds can be intercalated into LDHs through anion exchanges, giving rise to functional materials with characteristic optical properties or photochemical behaviors.[46−52] Especially, LDHs have been speculated as a possible inorganic catalyst for the origin of organic life.[53,54] It has been supposed, through anion exchanges, that phosphates entering the interlayer of LDHs on the primitive Earth became concentrated, favoring the subsequent synthesis of polyphosphate, the proto-biomolecules.[53]

Anions and water influence properties of LDHs through interacting with rigid brucite-like layers. Depending on water content and the composition of anions and cations, rigid layers exhibit characteristics such as swelling,[36,55] undulations,[56] and polytype-transformations.[57,58] Polytypism, referred to as one-dimensional polymorphism, accounting for different layer-stacking ways, is a characteristic property of layered inorganic compounds.[59−62] Polytypes are coined based on the space-group symmetry and number of layers in a minimal repeating unit. Reported polytypes for LDHs are $1T$ (one-layer trigonal polytype), $2H_1$ (two-layer hexagonal polytype), $3R_1$ (three-layer rhombohedral polytype), $3R_2$ (another three-layer rhombohedral polytype), etc.[63] Detailed characterizations of different polytypes will be shown in Section 2.2. LDHs intercalated with CO_3^{2-} generally exhibit $3R_1$ and $2H_1$ polytypes,[3,64−66] while those with Cl^- were just reported to be of a $3R_1$ polytype.[67,68] The polytype of LDHs intercalated with SO_4^{2-} depends on cation ratio and water content.[69] For instance, zincowoodwardite $(Zn_{1-x}Al_x)(OH)_2(SO4)_{x/2}\cdot nH_2O$ exists as a $1T$ polytype when x ranges from 0.32 to 0.33, while it exists as a $3R_1$ polytype when x ranges from 0.35 to 0.50.[70] In another instance, honessite and hydrohonessit are two mineral species with almost the same chemical formula $([Ni_6Fe^{III}_2(OH)_2](SO_4)\cdot mH_2O)$ except that water content m is higher in the latter.[71] Honessite was suggested to be a $3R_1$ polytype,[58] while hydrohonessit was thought to be a $1T$[72] or $3R_2$ polytype.[58] How is a polytype determined by the water content and composition of cations and anions? What is the relationship between the layer-stacking way and local coordination structures of anions and water? These remain as questions which we will explore in this article.

The reported polytypes were characterized by powder X-ray diffraction (XRD) patterns.[3,60,69,73] However, there has been uncertainty in determining a polytype, because there are stacking faults, turbostratic distortions, and intergrowths of different polytypes in LDHs.[74] Through building structural models of polytypes, simulating the XRD patterns and comparing them with observed ones, reliable polytype attributions can be obtained.[60,61,69,75] However, there is still doubt about the artificially chosen structural models, which raise a question: Could different models lead to similar XRD patterns? On the other hand, there have been discrepancies in explaining configurations of intercalated anions through experiments. For example, NO_3^- anions in LDHs with a high basal spacing were suggested to be "stick-lying"[76] or "tilt-lying"[77,78] based on different experimental observations. Molecular dynamics (MD) simulations seem promising in verifying experimental results. In principle, if a simulation is long enough, thermodynamically stable polytype structure can be achieved independent of the initial model. In this study, we use the simulated-annealing[79] method in order to accelerate the equilibration process. MD simulations could be performed with ab initio methods[29,35,80,81] or empirical force fields.[27,28,31,82] Because the later requires much less computational power, it is superior in predicting polytype-transition behaviors. Although interlayer swelling and the structure of water and anions have been investigated in previous simulation studies,[27−29,31,35,80−82] the dependence of polytype on compositions has not been disclosed explicitly to our knowledge. In this paper, we give a detailed and clear picture of the polytype-transition and interlayer-swelling behaviors and their relationship with compositions of water, anions, and cations. Through comparing our results with available experimental observations, they are in general agreement. Moreover, since simulations are performed with continuous water contents, how a polytype transition is induced or not is shown through the variation of the coordination structure of water or anions. Not only a more detailed picture compared to experimental observations is provided here, but also the factors determining a polytype are pointed out. We deduce a polytype is collectively determined by the local coordination structure and long-ranged Coulombic interactions. The local coordination structure is formed due to hydrogen bonds (HB) between anions, water, and layers, i.e., short-ranged electrostatic interactions. The clarification of polytypism paves the way for understanding the relationship between stability of LDHs in environment and their microscopic structure. It also sheds light on synthesizing materials derived from LDHs through anion exchanges or exfoliation. Intercalating large organic compounds[46] or delamination[83] requires increasing the interlayer spacing at first, which is probably more appropriate for LDHs with NO_3^- or SO_4^{2-}. As will be shown in this paper, LDHs with those anions exhibit interlayer swelling and a polytype transition with increasing water content, which correlates with the flexible coordination structure of anions.

In this study, LDHs intercalated with CO_3^{2-}, NO_3^-, SO_4^{2-}, and Cl^- anions are investigated independently, with continuous water contents and the most reported cation ratios (M^{II}:M^{III} = 3:1 and 2:1).[63] M^{II} and M^{III} are Mg^{2+} and Al^{3+}, respectively, corresponding to the most common type of LDHs.[63] It is expected the results of this study can be extended to LDHs comprised by other cations with similar charges and radii. Results of our study and comparisons with experiments are shown in Section 3. Swelling and polytype-transition behaviors are relevant to local coordination structure and long-ranged Coulombic interactions, which will be discussed in Section 4. Through disclosure of the relationship between the structure and chemical composition of LDHs, its implication to their stability will also be discussed.

2. METHODOLOGY

2.1. Simulation Details. The chemical formulas of LDHs we study are $Mg_{2/3}Al_{1/3}(OH)_2(A^{n-})_{1/(3n)}\cdot mH_2O$ and $Mg_{3/4}Al_{1/4}(OH)_2(A^{n-})_{1/(4n)}\cdot mH_2O$, where A^{n-} is CO_3^{2-}, NO_3^-, SO_4^{2-}, or Cl^-. In this article, systems with Mg:Al = 2:1 are designated as LDH-2/1-CO_3, LDH-2/1-NO_3, LDH-2/1-SO_4, and LDH-2/1-Cl, respectively, while those with Mg:Al = 3:1 are LDH-3/1-CO_3, LDH-3/1-NO_3, LDH-3/1-SO_4, and LDH-3/1-Cl, respectively. Initial layer structures of all the simulated systems are based on the same $3R_1$-hydrotalcite

DOI: 10.1021/acs.inorgchem.8b00949
Inorg. Chem. 2018, 57, 7299−7313

model, whose crystal structure was determined experimentally exhibiting rhombohedral ($R\bar{3}m$) symmetry.[73] A complete Mg/Al ordered arrangement (Figure 1)[84,85] is assumed for all the

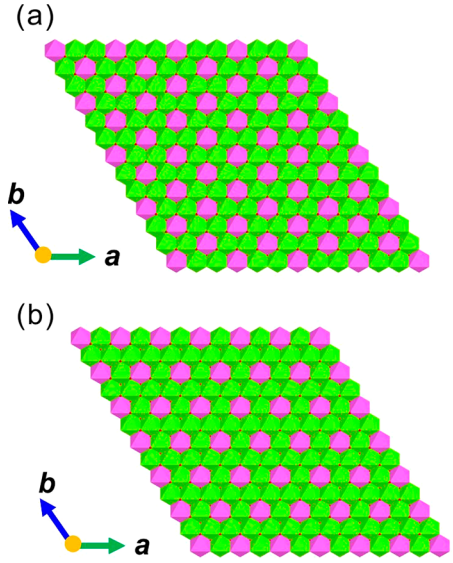

Figure 1. Top view of layers of LDHs, whose ratios of Mg/Al are 2:1 (a) and 3:1 (b). Al and Mg octahedra are in purple and green, respectively.

layers. For convenience, hexagonal instead of rhombohedral unit cells are built, with $a = b = 3.05$ Å and $c \approx 30$ Å. As compared to the reported crystal structure,[73] the interlayer space along the c axis has been enlarged for the convenience of inserting anions and water molecules. A model consists of 12 × 12 × 2 unit cells in a, b, and c directions, respectively. Water molecules and anions are inserted into interlayer galleries based on corresponding chemical formulas. The investigated water contents (m) are listed in Table 1. Although m is assumed a

Table 1. Investigated Water Content m and Initial Coupled Temperature T_i for LDHs Intercalated with Different Anions

intercalated anion	m	T_i (K)
CO_3^{2-}	0.33–0.97	600
NO_3^-	0.22–0.83	500
SO_4^{2-}	0.64–1.67	500
Cl^-	0.22–0.83	450

priori, the correspondence between simulated and experimental systems can be justified a posterior through comparing basal spacings, which will be shown in the Results. Periodic boundary conditions are applied in all directions. Simulations are performed with LAMMPS.[86] The ClayFF force field[87] with SPC water model[88] incorporated is used to describe interactions between atoms in the layers and intercalated water. According to Wang et al., the partial charges of O atoms in the layers are modified to make models electrostatically neutral (−0.9742 |e| while Mg/Al = 2/1 and −1.0069 |e| while Mg/Al = 3/1 vs −0.9500 |e| in the original force field).[27,89] The force fields for CO_3^{2-}, NO_3^-, SO_4^{2-}, and Cl^- anions are according to Wang and Becker,[90] Baaden et al.,[91] Williams et al.,[92] and Cygan et al.,[87] respectively. Long-range electrostatic interactions are described by the particle–particle particle–mesh (PPPM) method.[93] Short-range Lennard-Jones interactions are cut off at 15.0 Å. The time step is 0.5 fs. We aim at revealing properties of LDHs at ambient temperature (300 K) and pressure (1 atm). Before performing isothermal–isobaric-ensemble (NPT) simulations in such conditions, the method of simulated annealing[79] is applied, in order to efficiently optimize structure. A system is set to a higher temperature (T_i) at the beginning and then annealed to 300 K in 3 ns through linearly scaling coupled temperature with time. T_i should be high enough for avoiding being trapped in local energy-minimum states, but it cannot be too high to lead to structure breakdown. T_i for different systems are listed in Table 1. During the annealing, the Berendsen thermostat[94] is used to couple temperature, because it is efficient in approaching target temperature. The Parrinello–Rahman barostat[95,96] is used to couple pressure through scaling each dimension of the supercell independently. After annealing, NPT simulations are performed at ambient temperature and pressure for 2 ns. In this stage, the Nosé–Hoover thermostat,[97,98] which generates the expected thermodynamic ensemble,[99] is used to couple temperature. Data are saved every 0.1 ps in the last 1.5 ns simulation for analysis.

Polytype transitions with variation in water content appear in the systems intercalated with NO_3^- and SO_4^{2-}, which will be shown in the Results. In order to verify if the polytype transition depends on initial structure, simulations are also performed with 1T-polytype LDHs as initial models using the same methods (Section S2 in the Supporting Information). The 1T polytype is built through translating layers in a $3R_1$ polytype. The difference between polytypes will be described in the next section.

2.2. Polytype Classification. 1T, $2H_1$, $3R_1$, and $3R_2$ are polytypes reported in the literature.[58,63,69] In the name of a polytype, the former number stands for the number of layers in a unit cell, while the letter is the initial of the name of the lattice or crystal system (Table 2). The optional subscript number is used to separate different polytypes with the same periodicity and belonging to the same lattice and crystal systems. It should be noted the 1T polytype coined by Mills et al.[63] had been referred to as a 1H polytype by Bookin and Drits,[57] because it belongs to the trigonal crystal system and the hexagonal lattice system at the same time. In this paper, we use the name 1T.

Table 2. Characterizations of $3R_1$, $3R_2$, and 1T Polytypes

polytype	space group	crystal/lattice system	interlayer type	displacement vector
$3R_1$	$R\bar{3}m$	Trigonal/Rhombohedral	P	0
$3R_2$	$R\bar{3}m$	Trigonal/Rhombohedral	O_1	$\frac{2}{3}\vec{\mathbf{a}} + \frac{1}{3}\vec{\mathbf{b}}$;[a] $-\frac{1}{3}\vec{\mathbf{a}} + \frac{1}{3}\vec{\mathbf{b}}$; $-\frac{1}{3}\vec{\mathbf{a}} - \frac{2}{3}\vec{\mathbf{b}}$
1T (1H)	$P\bar{3}m1$	Trigonal/Hexagonal	O_2	$\frac{1}{3}\vec{\mathbf{a}} + \frac{2}{3}\vec{\mathbf{b}}$; $\frac{1}{3}\vec{\mathbf{a}} - \frac{1}{3}\vec{\mathbf{b}}$; $\frac{1}{3}\vec{\mathbf{a}} + \frac{2}{3}\vec{\mathbf{b}}$

[a] $\vec{\mathbf{a}}$ and $\vec{\mathbf{b}}$ are primitive vectors of the unit cell in the a and b directions, respectively.

DOI: 10.1021/acs.inorgchem.8b00949
Inorg. Chem. 2018, 57, 7299–7313

The $2H_1$ polytype, though appearing in nature, e.g., as manasseite inside hydrotalcite, was rarely found in synthetic experiments at ambient conditions.[74] It was reported the $2H_1$ polytype appears at ca. 1.5 GPa.[100] The intergrowth of $2H_1$ and $3R_1$ polytypes has also been deduced to be kinetics.[59] The $2H_1$ polytype was also found in gibbsite-derived $LiAl_2$-LDHs.[61] Since our simulations are for brucite-derived LDHs and performed at ambient conditions, the appearance of a $2H_1$ polytype is not expected. The differences between $3R_1$, $3R_2$, and $1T$ polytypes are shown in Figure 2 and Table 2. With regard to a specific polytype, the hydroxyl (OH) sheet stacking is the same in each interlayer. The $3R_1$ polytype exhibits a *P*-type interlayer,[57] in which OH groups form prisms (Figure 2d). The $3R_2$ and $1T$ polytypes all exhibit *O*-type interlayers,[57] where OH groups form octahedra (Figure 2e,f). The octahedra of the $3R_2$ and $1T$ polytypes, respectively, are mirror images of each other. As to distinguish them, the interlayer types are named O_1- and O_2-type, respectively. The differences between interlayer types are displacements between adjacent OH sheets. There is no displacement between sheets in an ideal *P*-type interlayer (Figure 2g). For the *O*-type interlayer, the minimal displacements for the lower OH sheet to coincide with the upper one on the ***ab*** plane lie in three directions (Figure 2h,i). The displacement vectors are exhibited in Table 2. In $3R_1$, $3R_2$, and $1T$ polytypes, there is no layer inversion. Thus, the displacements between adjacent sheets in an interlayer are enough for distinguishing different polytypes. The displacement vectors are derived through analyzing simulation results as follows. First, for an O_{OH} (hydroxyl O) atom in the lower OH sheet, in the range of the inscribed circle of the hexagon made up of 6 nearest-neighbor O_{OH} atoms (Figure 2g,h,i), we search for the projection of an O_{OH} atom from the upper sheet in the four sectors on the ***ab*** plane, respectively. Then, the vector between the O_{OH} atom in the lower sheet and the projection of that from the upper one is calculated. In each sector of the ***ab*** plane, the vector is averaged for every O_{OH} atom from the lower sheet over all the frames saved in the production simulation. Results will be shown in Section 3 (Figure 3a,d, 7a,d, 9a,d, 11a,d). It should be noted that, this calculation is based on the assumption of a perfect hexagonal arrangement made up of OH groups in a sheet. However, for a cation-ordered layer which is the case of this study, the distance between OH groups is heterogeneous, and thus the arrangement is not perfectly hexagonal.[101] And yet, taking the space average into account, on average an OH group is in a perfect hexagonal environment. Thus, since the displacement vector is averaged over all O_{OH} atoms, the local nonhexagonal arrangement makes no difference on the result. More details on this issue can be seen in Section S1 of the Supporting Information.

We note that if the cation order is taken into account, the three-layer polytype of rhombohedral symmetry ($3R_1$ or $3R_2$) is actually a one-layer polytype of monoclinic symmetry.[101] This

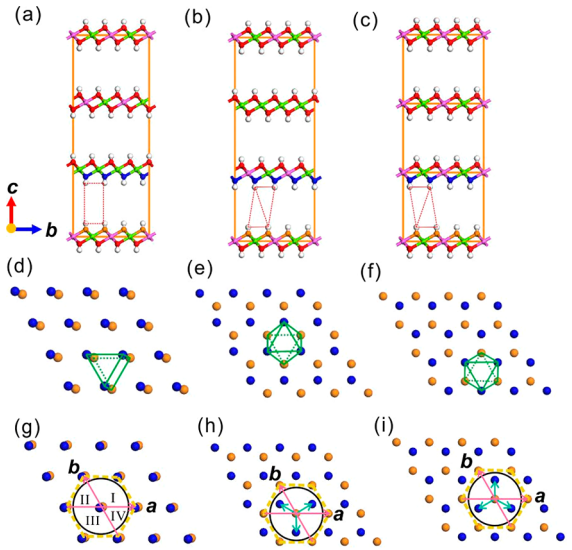

Figure 2. Side views of $3R_1$(a), $3R_2$(b), and $1T$(c) polytypes. Top views of interlayers composed of OH sheets of $3R_1$(d), $3R_2$(e), and $1T$(f) polytypes, which exhibit *P*-, O_1-, and O_2-type sheet stackings, respectively. Schematics of displacements between adjacent sheets of *P*- (g), O_1- (h), and O_2-type (i) interlayers on the ***ab*** plane. Al, Mg, O, and H atoms are in purple, green, red, and white, respectively. O atoms of the lower sheet of the interlayer are in orange, while those of the upper one are in blue.

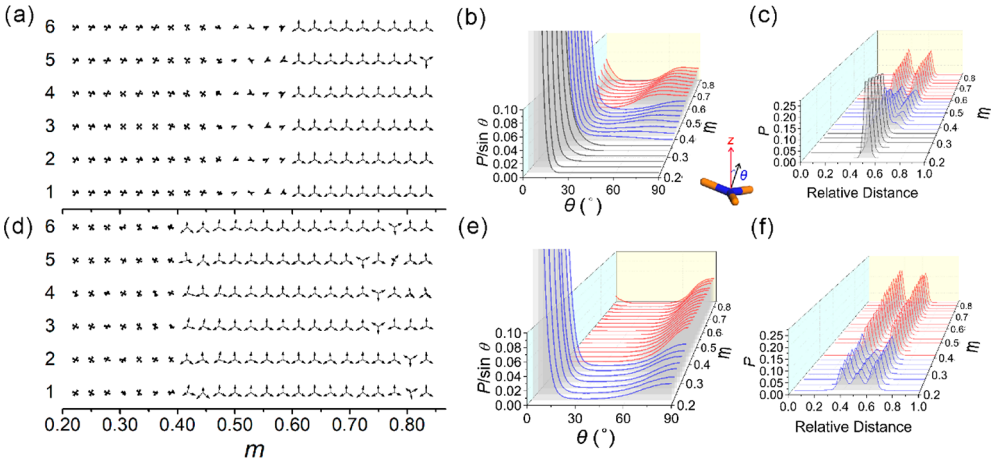

Figure 3. Structure of layers, intercalated NO_3^- anions, and water. (a) Displacement vectors between adjacent OH sheets in different interlayers of LDH-3/1-NO_3 as a function of water content *m*. The six interlayers are numbered and marked on the left. (b) Probability distribution of tilt angle θ normalized by sin θ as a function of *m* for LDH-3/1-NO_3. (c) Probability distribution of water O atoms in the interlayer gallery as a function of *m* for LDH-3/1-NO_3. (d), (e), and (f) are the same as (a), (b), and (c), respectively, except the system is LDH-2/1-NO_3.

DOI: 10.1021/acs.inorgchem.8b00949
Inorg. Chem. 2018, 57, 7299−7313

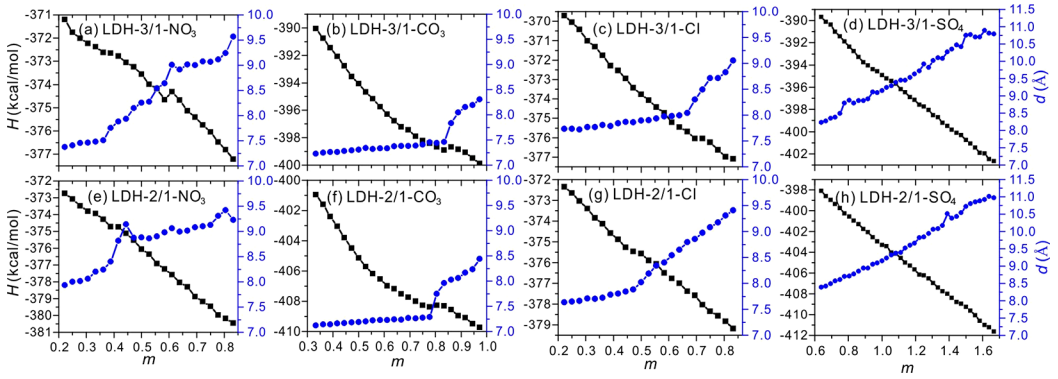

Figure 4. Enthalpy H and basal spacing d of the systems as a function of water content m.

description does not change the fact of layer stacking. In this paper, we still use the names $3R_1$ and $3R_2$ to describe polytypes ignoring cation order, in order to be in accord with more literature.[63]

3. RESULTS

3.1. LDHs with NO_3^-. For LDHs intercalated with NO_3^- anions, the variation of average displacement vectors with water content m shows a phase transition from a $3R_1$ to $1T$ polytype (Figure 3a,d). For an ideal $3R_1$ polytype, all the interlayers are P types (Figure 2g), and thus there is no displacement between OH sheets. However, due to thermal fluctuation, there would be a slight displacement in each sector on average. These are observed in cases with lower m. As m increases over 0.60 for LDH-3/1-NO_3 (Figure 3a) or 0.40 for LDH-2/1-NO_3 (Figure 3d), the displacement vectors show all the interlayers become O_2-type ones, i.e., a transition into a $1T$ polytype. Such a phase transition is almost independent of the initial model (Section S2 in Supporting Information). At much higher m, mixed-layer phenomena are observed, i.e., occasional appearances of O_1-type interlayers among O_2-type ones.

The phase transition is relevant to variations in basal spacings (d), NO_3 configurations, and water distributions with m. For LDH-3/1-NO_3, there are three stages of increments of d, i.e., $m < 0.37$, $0.37 < m < 0.60$, and $m > 0.60$ (Figure 4a). Only in the last stage the polytype is $1T$. During the first or last stages, variations of d with m are gentle, while in the intermediate stage, d exhibits a sharp increase. d varies in response to the configuration of NO_3^-, which is quantified by the distribution of tilt angle θ (Figure 3b). θ is defined as the angle between the z axis and the normal vector of the NO_3 plane. For $m < 0.37$, NO_3 planes are flat with respect to layers (Figure 5a,b); as shown in the distribution there is a sharp peak which locates at $\theta \approx 0$ and almost vanishes for $\theta > 45°$ (Figure 3b). In this stage, the coordination number (CN) of H_{OH} (hydroxyl H) atoms around O_N (nitrate O) atoms (CN (O_N–H_{OH})) is approximately 2.0 (Figure 6a, the derivation of CN can be seen in Section S3 of the Supporting Information); i.e., almost each O_N atom accepts two HBs from two opposite OH groups (Figure 5b). Thus, a NO_3^- ion exhibits a D_{3h} point group symmetry. For $0.37 < m < 0.60$, although the sharp peaks for $\theta \approx 0$ are still present, obvious distributions for $\theta > 45°$ appear (Figure 3b). This implies flat NO_3^- ions are accompanied by tilted ones, as shown in the snapshot (Figure 5d). Layer undulations are observed in this stage, which were also reported in a previous simulation study.[56] The highest point group symmetry for tilted NO_3^- ions is C_{2v}, as shown by two examples of tilted ions

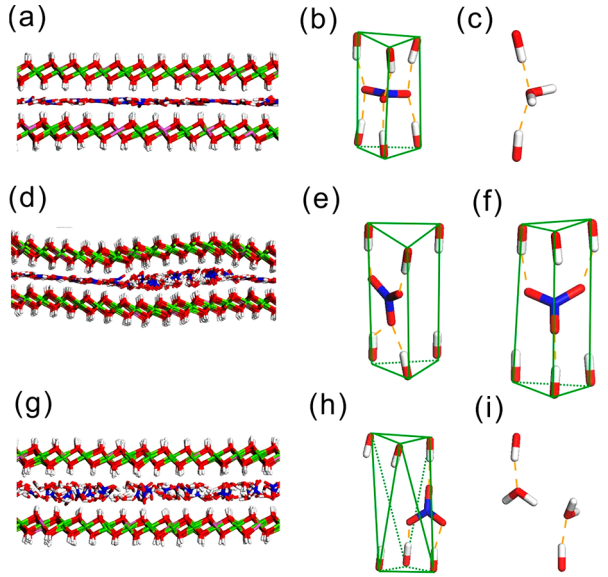

Figure 5. Snapshots of LDH-3/1-NO_3 with m = 0.33 (a, b, c), 0.50 (d, e, f), and 0.67 (g, h, (i). Flat (b) and tilted NO_3^- anions (e, f, h) with D_{3h} and C_{2v} point group symmetries, respectively, and water molecules coordinated by two opposite OH groups (c) and just by one OH group (i).

(Figure 5e,f). Each O_N atom accepts one or two HBs from OH groups. Thus, CN (O_N–H_{OH}) drops to between 1.0 and 2.0 in this stage (Figure 6a). The sharp increase of d with m in this stage is due to layer puckering because more NO_3^- ions are transformed into tilted configurations. After the $3R_1$-$1T$ transition, i.e., $m > 0.60$, the layer becomes flat again (Figure 5g). Tilted configurations of NO_3^- ions are predominant; as shown in the distribution the main peak locates at θ larger than 60° (Figure 3b). Such configurations with C_{2v} point group symmetries (Figure 5h) are favored in the O-type interlayer. Almost each O_N atom just accepts one HB as shown by CN (O_N–H_{OH}) being close to 1.0 (Figure 6a). Configurational transformations of anions correspond to changes in water distributions (Figure 3c). The probability distribution of a water molecule in an interlayer is calculated based on the relative distance of the molecule.[31] The distance between an O_w (water O) atom and the nearest O_{OH} atom of the lower layer is defined as r_1, while that between it and the nearest O_{OH} atom of the upper layer is defined as r_2. The relative distance is $r_1/(r_1 + r_2)$. For $m < 0.37$, in the distributions a sharp peak locates in the middle (Figure 3c), corresponding to a single water monolayer

DOI: 10.1021/acs.inorgchem.8b00949
Inorg. Chem. 2018, 57, 7299–7313

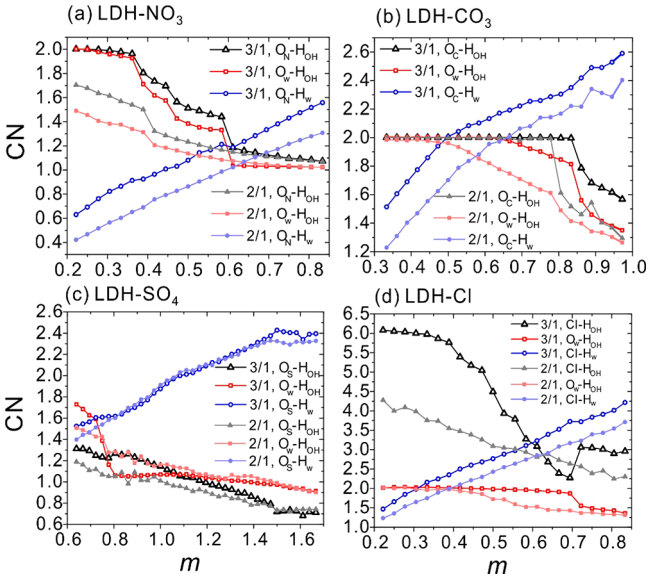

Figure 6. Coordination numbers (CN) as functions of water content m in different systems. The coordination atoms are hydroxyl H atoms (H_{OH}) and water H atoms (H_w), while the central atoms are nitrate O atoms (O_N), carbonate O atoms (O_C), sulfate O atoms (O_S), and Cl^- ions. Mg/Al ratios and coordination relations are marked in the legends.

(Figure 5a). In the monolayer, almost each water molecule accepts two HBs from two opposite OH groups (Figure 5c) as shown by CN (O_w–H_{OH}) ≈ 2.0 (Figure 6a). For 0.37 < m < 0.60, with part of NO_3^- ions being tilted, two smaller peaks appear in the left and ride sides of the middle one (Figure 3c), corresponding to the local bilayer in the distorted interlayer space (Figure 5d). During this stage, increasing water molecules just accept one HB from one layer, as shown by the decrement of CN (O_w–H_{OH}) (Figure 6a). After the polytype transition (m > 0.60), the middle peak disappears and the distribution is replaced by two symmetrical peaks (Figure 3c). They correspond to a full bilayer consisting of water molecules (Figure 5g), which just accept HBs from one layer (Figure 5i). This is also evident in CN (O_w–H_{OH}), which is close to 1.0 (Figure 6a).

For LDH-2/1-NO_3, two-stage variations of d with m are observed (Figure 4e), corresponding to the $3R_1$-1T transition (Figure 3d). Within this process, similar to the case of LDH-3/1-NO_3, NO_3^- ions transform from mainly flat to totally tilted configurations (Figure 3e). CN (O_N-H_{OH}) and CN (O_w-H_{OH}) exhibit obvious decreases during the transition (Figure 6a), approaching 1.0 with increasing m. The formation of a full water bilayer after the polytype transition is evident, as also shown in water distributions (Figure 3f).

The above results clearly show how the polytype transition and interlayer swelling are induced by the concerted variations of configuration and coordination structure of anions and water. The simulation results can be verified through comparing anionic configurations and interlayer spacings derived from experiments. During the transformation from flat to tilted configurations of NO_3^- ions, the point group symmetry of them is transformed from D_{3h} (Figure 5b) into C_{2v} (Figure 5e,f,h). NO_3^- ions with these symmetries were also reported in the studies of Fourier transform infrared spectra (FTIR).[39,76,77] The C_{2v} point group symmetry was ascribed to tilted NO_3^- ions by Wang et al.,[77] which was shown responsible for the increase in d, consistent with what we find here. However, Xu et al.[76] suggested the increase in d is due to "stick-lying" NO_3^- ions, which is not found here. Classical MD simulations and ab initio studies by others all showed tilted instead of "stick-lying" NO_3^- ions at higher basal spacings,[26,35,78] consistent with our results.

This study shows d varies from less than 8.0 Å to over 9.0 Å (Figure 4a,e) with m. This range of basal spacing is consistent with that revealed by XRD patterns of LDHs with M^{II}:M^{III} = 2:1.[76,78,102] Thus, the $3R_1$-1T evolution accompanying the variation in basal spacing, though it has not been reported, should be present in experiments for LDH-2/1-NO_3. However, the patterns of LDHs with M^{II}:M^{III} = 3:1 showed the highest basal spacing is more or less 8.5 Å, even at more than 80% relative humidity.[55,102] Based on the relationship between basal spacing and polytype (Figure 3a, 4a), such a spacing probably corresponds to the $3R_1$ state. We have shown a polytype transition happens at a much higher water content for the system with Mg:Al = 3:1, so that probably such a high content is never met at the experimental humidity. Thus, 1T LDH-3/1-

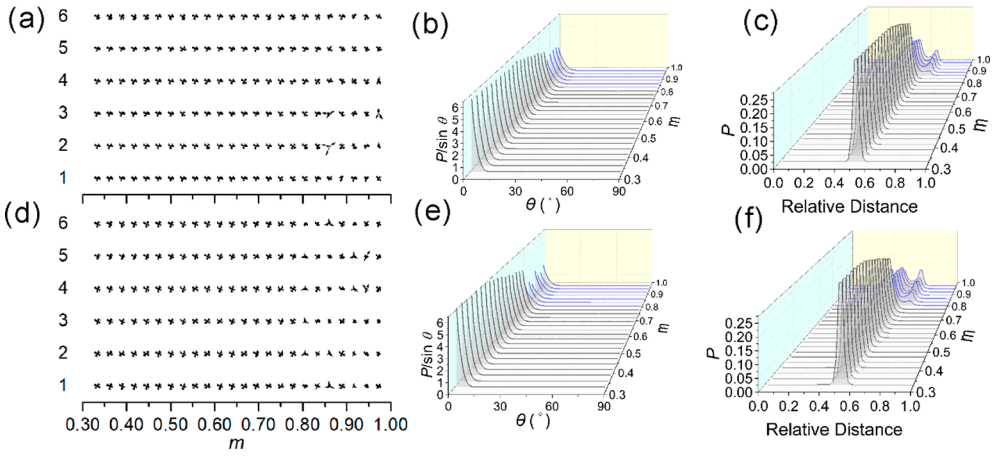

Figure 7. Structure of layers, intercalated CO_3^- anions, and water. (a) Displacement vectors between adjacent OH sheets in different interlayers of LDH-3/1-CO_3 as a function of water content m. The six interlayers are numbered and marked on the left. (b) Probability distribution of tilt angle θ normalized by sin θ as a function of m for LDH-3/1-CO_3. (c) Probability distribution of water O atoms in the interlayer gallery as a function of m for LDH-3/1-CO_3. (d), (e), and (f) are the same as (a), (b), and (c), respectively, except the system is LDH-2/1-CO_3.

DOI: 10.1021/acs.inorgchem.8b00949
Inorg. Chem. 2018, 57, 7299–7313

NO_3 probably does not exist in experiments. In addition, for LDHs intercalated with NO_3^- with much higher M^{II}:M^{III} ratio (e.g., 4:1), the basal spacing was observed to be much lower, i.e., just slightly over 8.0 Å.[55,76,78] It is reasonable, as we have found with a higher M^{II}:M^{III} ratio flat configurations of NO_3^- ions do not change until above a much higher water content. This high water content is hardly met at the experimental humidity. There are three stages of basal-spacing variations with m for LDH-3/1-NO_3, i.e., $3R_1$ polytype with flat NO_3^- ions, $3R_1$ polytype with both flat and tilted NO_3^- ions, and $1T$ polytype with tilted NO_3^- ions. For LDH-2/1-NO_3, only the latter two stages are observed here. Based on XRD patterns through hydration and dehydration experiments, Jobbágy et al. suggested NO_3^- ions are not simply transformed from purely flat to tilted configurations during the interlayer expansion, but an intermediate stage is present.[55] Such an intermediate stage is consistent with the stage with both flat and tilted NO_3^- ions we find here.

Thermodynamically, a phase transition is associated with variation in enthalpy H. H is calculated with the equation: $H = U + pV$, where U is the total potential energy of the system, p the pressure, and V the volume. The kinetic energy is neglected in the calculation of H, because it is linear with atomic number at constant temperature. H is normalized by $12 \times 12 \times 6$, so as to represent the enthalpy per interlayer in a unit cell. For LDH-3/1-NO_3, an abrupt increase in H is observed as the phase transition happens (Figure 4a), implying the higher configurational energy of the $1T$ polytype. For LDH-2/1-NO_3, a small plateau is observed corresponding to the polytype transition (Figure 4e).

3.2. LDHs with CO_3^{2-}. For LDHs intercalated with CO_3^{2-} ions, the displacement vectors show all the interlayers are P-types, irrespective of water content or Mg/Al ratio (Figure 7a,d). The $3R_1$ polytype is maintained throughout all the water contents investigated, though d increases dramatically when m exceeds 0.84 for LDH-3/1-CO_3 (Figure 4b) or 0.78 for LDH-2/1-CO_3 (Figure 4f). This transition corresponds to the kink in the enthalpy line, which implies a structural transformation. Snapshots show that before the transition point, a single monolayer consisting of water and anions lies in the interlayer gallery (Figure 8a), while after that, a coexistence of monolayer and bilayer is found (Figure 8d). The layers are transformed from flat to puckering ones. Such a transition is evidenced in the transformation of water distributions, where two small peaks appear beyond the middle one (Figure 7c,f). In the monolayer, a CO_3^{2-} ion accepts 6 HBs from layers (Figure 8b). In other words, each O_C (carbonate O) atom accepts two HBs from two opposite OH groups. This is reflected in CN of H_{OH} around O_C atoms (CN (O_C-H_{OH})), which is approximately 2.0 at lower water contents (Figure 6b). In the bilayer, a CO_3^{2-} ion just accepts HBs from one layer (Figure 8e). Thus, after the transition into a coexistence of monolayer and bilayer, CN (O_C-H_{OH}) decreases sharply (Figure 6b), but it is still higher than 1.0 due to the existence of a local monolayer. Unlike NO_3^- ions which exhibit tilted configurations at higher water contents, CO_3^{2-} ions are always predominantly flat, as shown by the sharp peak at $\theta \approx 0$ in the distributions (Figure 7b,e). This is the result of the coordination structure. Before the formation of a bilayer, CO_3^{2-} ions exhibit a D_{3h} point group symmetry (Figure 8b) as for NO_3^- ions at lower water contents. However, within the bilayer, the highest point group symmetry of CO_3^{2-} ions is C_{3v} (Figure 8e), unlike that of NO_3^- ions at higher water contents. As to water molecules, for m less than 0.64 for LDH-3/1-CO_3 or less than 0.50 for LDH-2/1-CO_3, CN (O_w-H_{OH}) is approximately 2.0 (Figure 6b), implying a water molecule is accepting two HBs from two opposite OH groups (Figure 8c). As m increases over 0.64 for LDH-3/1-CO_3 or 0.50 for LDH-2/1-CO_3, CN (O_w-H_{OH}) decreases, implying part of the water molecules become just accepting HBs from one layer. Further increase of m leads to the observation of another inflection point of CN (O_w–H_{OH}), which corresponds to the transition point of CN (O_C–H_{OH}), reflecting the bilayer formation.

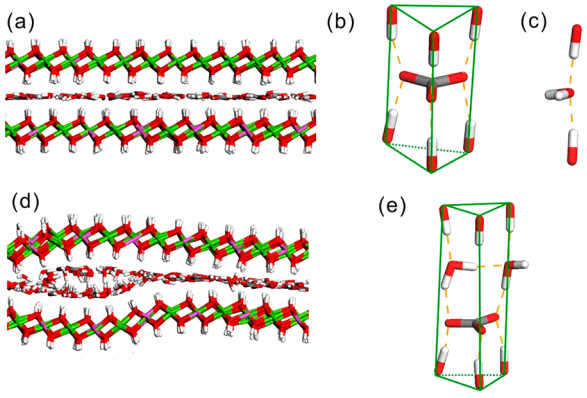

Figure 8. Snapshots of LDH-3/1-CO_3 with m = 0.50 (a, b, c) and m = 0.97 (d, e). CO_3^{2-} anions and water molecules accepting HBs from two layers (b, c) and just from one layer (e).

Hydration studies showed the increment of the basal spacing of LDHs with CO_3^{2-} is less than 0.1 Å even when the relative humidity is increased to 100%.[36,102] This corresponds to the behavior of simulated ones before the bilayer formation. Thus, a bilayer should not be present in experimental conditions and LDHs with CO_3^{2-} are nonswelling. The coordination structure of CO_3^{2-} ions (Figure 8b) in the monolayer we disclose is consistent with the ab initial result with m = 0.66[35] and that supposed by Taylor.[64,103] Thus, each CO_3^{2-} ion occupies three OH sites. On the other hand, a water molecule occupies one site accepting two opposite HBs (Figure 8c). Assuming all the OH sites are occupied by CO_3^{2-} ions and water molecules, Miyata suggested m is $1 - 3x/2$ for the formula $Mg_{1-x}Al_x(OH)_2(CO_3)_{x/2}\cdot mH_2O$.[104] Therefore, m is 0.625 for LDH-3/1-CO_3 and 0.500 for LDH-2/1-CO_3, respectively, more or less corresponding to the first inflection points of CN (O_w-H_{OH}) shown here (Figure 6b). Natural LDHs with CO_3^{2-} were reported to be with even lower m values.[63] Our study now shows, with m equal to or smaller than such values, CO_3^{2-} ions and water exhibit tightly coordination structure in the interlayer gallery. At the hypothetic high water content, the layer puckering needs a large energy cost, as shown by the kink in the enthalpy line (Figure 4b,f). This probably leads to the nonswelling behavior of LDHs with CO_3^{2-}.

3.3. LDHs with SO_4^{2-}. The displacement vectors show the polytypism exhibits a three-stage characteristic for LDHs intercalated with SO_4^{2-} ions (Figure 9a,d). The simulated polytype transition is almost independent of the initial model (Section S2 in Supporting Information). For LDH-3/1-SO_4, when m is less than 0.76 or larger than 1.48, almost all the interlayers belong to P-types, representing $3R_1$ polytypes. With intermediate m values, interlayers are a mixture of O_1- and O_2-types with comparable amounts. The enthalpy line does not exhibit distinct variations corresponding to polytype transitions

DOI: 10.1021/acs.inorgchem.8b00949
Inorg. Chem. 2018, 57, 7299−7313

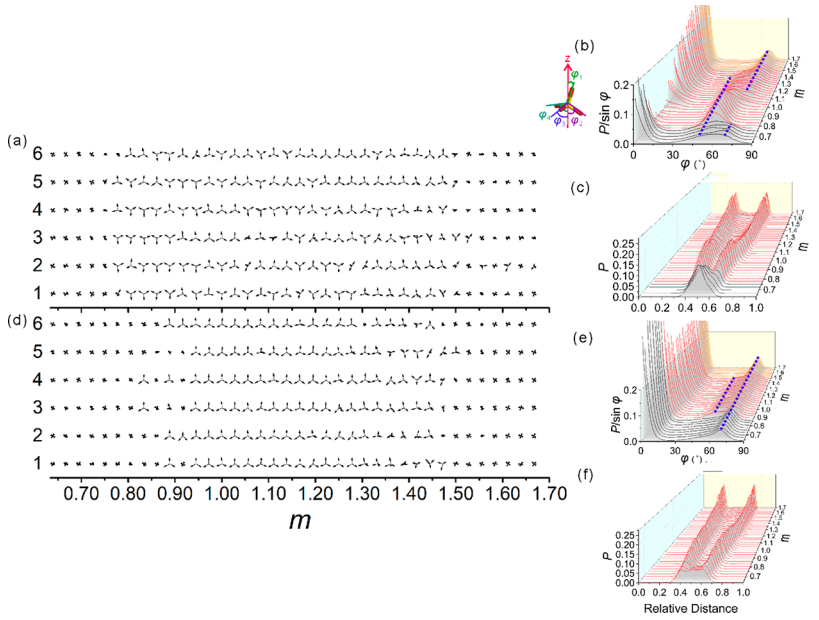

Figure 9. Structure of layers, intercalated SO_4^{2-} anions, and water. (a) Displacement vectors between adjacent OH sheets in different interlayers of LDH-3/1-SO_4 as a function of water content m. The six interlayers are numbered and marked on the left. (b) Probability distribution of angle φ normalized by sin φ as a function of m for LDH-3/1-SO_4. (c) Probability distribution of water O atoms in the interlayer gallery as a function of m for LDH-3/1-SO_4. (d), (e), and (f) are the same as (a), (b), and (c), respectively, except the system is LDH-2/1-SO_4.

(Figure 4d), implying the energy variation is negligible during the transition. However, large increments of d are observed around m = 0.76 and 1.48 (Figure 4d), correlated to transformations of SO_4^{2-} configurations. When m < 0.76 and LDHs exhibit $3R_1$-polytype structure, most SO_4^{2-} ions show a C_{3v} point group symmetry (Figure 10b), accompanied by some exhibiting a C_s point group symmetry (Figure 10c). The C_s configuration seems unstable as it leads to the distortion of the prism structure. The O_S (sulfate O) atom of a C_{3v} SO_4^{2-} ion accepts 1.5 HBs from OH groups on average (Figure 10b), while that of a C_s ion accepts 1.25 HBs (Figure 10c). During the stage of m < 0.76, CN (O_S-H_{OH}) is more or less in the range between 1.30 and 1.25 (Figure 6c), reflecting the existences of those two configurations. Configurations of SO_4^{2-} ions are quantified by the distribution of φ (Figure 9b), which is defined as the included angle between the line the S−O bond lies in and that the z axis lies in. With m lower than 0.76, as shown by black lines, the distributions are made up of three peaks locating at around φ = 0°, 55°, and 70°. Peaks at 0° and 70° correspond to C_{3v} configurations, while that at 55° is for the C_s configuration. As m increases over 0.76 and interlayers become *O*-types, the peaks for C_{3v} configurations almost vanish, while that for C_s configurations becomes dominant. This reveals the C_s point group symmetry is favored at this stage. A snapshot shows now the SO_4^{2-} ion with a C_s point group symmetry is fixed in the octahedral cell consisting of OH groups (Figure 10e). Such a configurational transformation correlates with layer displacements and a large increment of d (Figure 4d). At much higher water contents, configurations with a C_{3v} point group symmetry reappear (Figure 10f,g,i), as shown by the reappearance of peaks at around 0° and 70° (Figure 9b). For m > 0.76 but <1.48, CN (O_S-H_{OH}) decreases with m, due to increasing C_{3v} SO_4^{2-} ions accepting less HBs from OH groups (Figure 10f,g). With m larger than 1.48, accompanying the backward transformation into a $3R_1$ polytype, the peak for C_s symmetry vanishes (Figure 9b). In this stage, a full bilayer consisting of water and anions in the interlayer gallery is observed (Figure 10h). The basal spacing becomes stable (Figure 4d), and so as CN (O_S−H_{OH}), which is approximately 0.75 (Figure 6c), reflecting the predominance of the C_{3v} SO_4^{2-} ions shown in the snapshot (Figure 10i). As to intercalated water, it has turned into a bilayer after the first transition from *P*- to *O*-type interlayers (Figure 9c). Such a transformation is also evidenced in the sharp decrease of CN (O_w-H_{OH}), which becomes close to 1.0 after the transformation (Figure 6c). CN of H_w (water H) atoms around O_S atoms (CN(O_S-H_w)) increases with m, implying SO_4^{2-} ions are more coordinated by water, but it becomes almost invariant when m is larger than

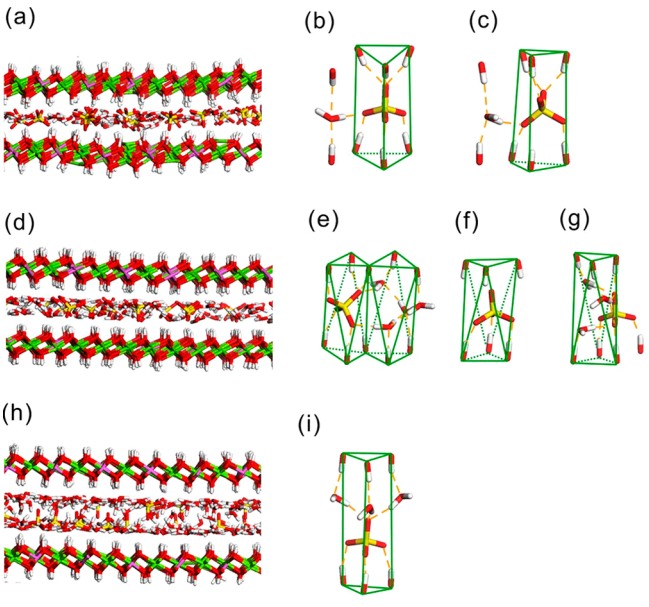

Figure 10. Snapshots of LDH-3/1-SO_4 with m = 0.67 (a, b, c), m = 0.89 (d, e), m = 1.00 (f, g), and m = 1.64 (h, i). SO_4^{2-} anions with C_{3v} (b, f, g, i) and C_s (c, e) point group symmetries.

DOI: 10.1021/acs.inorgchem.8b00949
Inorg. Chem. 2018, 57, 7299−7313

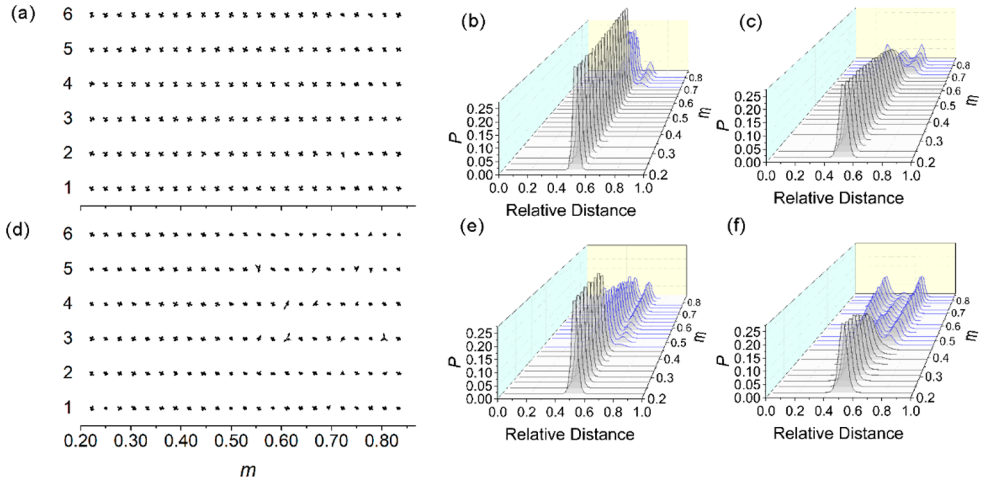

Figure 11. Structure of layers, intercalated Cl^- anions, and water. (a) Displacement vectors between adjacent OH sheets in different interlayers of LDH-3/1-Cl as a function of water content *m*. The six interlayers are numbered and marked on the left. (b) Probability distribution of Cl^- anions in the interlayer gallery as a function of *m* for LDH-3/1-Cl. (c) Probability distribution of water O atoms in the interlayer gallery as a function of *m* for LDH-3/1-Cl. (d), (e), and (f) are the same as (a), (b), and (c), respectively, except the system is LDH-2/1-Cl.

1.48 (Figure 6c). It implies in the second $3R_1$-polytype stage at high water contents a stable coordination structure between SO_4^{2-} ions, water, and layers is achieved.

For LDH-2/1-SO_4, $3R_1$-1*T* and 1*T*-$3R_1$ transitions are observed at around m = 0.82−0.93 and m = 1.50 (Figure 9d). Almost all the interlayers are O_2-types in the intermediate stage, corresponding to a 1*T* polytype, in contrast with the mixture of O_1- and O_2-type interlayers in the case of LDH-3/1-SO_4. According to the distributions of φ, peaks at around 0° and 70° for a C_{3v} point group symmetry are always predominant (Figure 9e). Shoulders at φ = 55° for a C_s point group symmetry are apparent in the intermediate stage, i.e., when the polytype is 1*T*. Thus, a C_s point group symmetry is characteristic of the *O*-type interlayers, as in the case of LDH-3/1-SO_4. In the second $3R_1$ stage at high water contents, CN (O_S−H_{OH}), CN (O_S−H_w), and CN (O_w−H_{OH}) are all almost invariant with *m* and exhibit similar values as in the case of LDH-3/1-SO_4 (Figure 6c). On the other hand, *d* is also less variant in the second $3R_1$ stage (Figure 4h). Thus, a similar bilayer structure consisting of well-coordinated C_{3v} SO_4^{2-} ions and water in the interlay gallery as in LDH-3/1-SO_4 (Figure 10h) is evidenced. However, unlike in the case of LDH-3/1-SO_4, the sharp decrease of CN (O_w−H_{OH}) (Figure 6c) and the formation of a water bilayer (Figure 9f) take place before the first $3R_1$−1*T* transition. Thus, the polytype structure is more correlated to the coordination of SO_4^{2-} ions than that of water.

Hydration and dehydration experiments showed the basal spacing of LDHs with SO_4^{2-} ranges from 8.0 to 11.0 Å,[36,102,105] consistent with our results (Figure 4h). Radha et al. found, for LDHs (Zn_2Cr-SO_4), with relative humidity increased from 0% to 100%, $3R_1$, 1*T*, and a new $3R_1$ phase appear in sequence, with basal spacings of 8.55 Å, 8.95 Å, and 10.9 Å, respectively.[105] This is in accord with the relationship between spacing and polytype we disclose (Figures 4h and 9d). The hydration and dehydration study by Iyi et al. showed LDHs (Mg_3Al-SO_4) exhibit a stepwise basal-spacing expansion from ca. 8.5 Å to 10.8 Å, and LDHs (Mg_2Al-SO_4) exhibit an expansion from ca. 9.0 Å to 11.0 Å, which probably imply transitions from mixed O_1- and O_2-type interlayers and a 1*T* polytype into $3R_1$ polytypes, respectively. The enthalpy lines we disclose are almost linear with *m*, and no kick or plateau is observed (Figure 4d,h). This reveals there is no energy barrier for polytype transition and interlayer expansion due to configurational adjustment of SO_4^{2-} ions, explaining the experimentally observed swelling behavior.

Through fitting XRD patterns, Radha et al. proposed SO_4^{2-} ions in LDHs (Zn_2Cr-SO_4) exhibit a C_{3v} point group symmetry. They also showed water and anions form bilayer structure when basal spacing is ca. 11 Å.[69] On the other hand, SO_4^{2-} ions with a configuration similar to the C_s point group symmetry shown here were suggested for bayerite-derived LDHs.[60] Thus, the configurations of SO_4^{2-} ions in our simulations are in general agreement with experimental results. Moreover, we find that in the intermediate stage with *O*-type interlayers, both C_{3v} and C_s point group symmetries coexist. And SO_4^{2-} ions with a C_s point group symmetry are deemed to be characteristic of this stage.

3.4. LDHs with Cl^-. For LDHs intercalated with Cl^- ions, no polytype transition is observed, as shown in displacement vectors which always exhibit $3R_1$-polytype characteristics (Figure 11a,d). We find a transition from a single monolayer consisting of anions and water (Figure 12a) into a coexistence of monolayer and bilayer (Figure 12b). Layer puckering is also

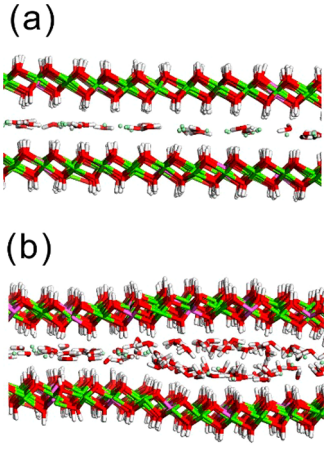

Figure 12. Snapshots of LDH-3/1-Cl with m = 0.22 (a) and m = 0.83 (d).

DOI: 10.1021/acs.inorgchem.8b00949
Inorg. Chem. 2018, 57, 7299−7313

observed, similar to the case of LDHs with CO_3^{2-}. Such a transition is evident in the variations of anion and water distributions (Figure 11b,c,e,f). The appearance of a bilayer more or less corresponds to the sharp increase in basal spacing and the plateau in the enthalpy line (Figure 4c,g). It is also evidenced in CN (O_w–H_{OH}), which decreases below 2.0 after the bilayer formation (Figure 6d). However, in the case of LDHs with CO_3^{2-} shown above, when CN (O_w–H_{OH}) becomes less than 2.0 a bilayer does not form immediately. A bilayer forms only after CN (O_C–H_{OH}) drops below 2.0, due to the determinant role CO_3^{2-} ions play in maintaining the single monolayer. In contrast, in the case of LDHs with Cl^-, since Cl^- ions exhibit flexible coordination as CN of H_{OH} atoms around Cl^- ions could vary from 2.5 to 6.0 in the studied range of m (Figure 6d), water coordination becomes more important in determining the interlayer structure.

XRD studies showed the basal spacing of LDHs with Cl^- is less than 8 Å under all humidity conditions and is almost nonexpandable.[36,102,104] This basal spacing corresponds to the stage with only a single monolayer of water and anions in the interlayer gallery (Figure 4c,g). The water molecule accepting two opposite HBs from two OH sheets is responsible for the stability of the monolayer and $3R_1$-polytype. The layer puckering at the hypothetic high water content sets an energy barrier forbidding the interlayer expansion, as in the case of LDHs with CO_3^{2-}.

4. DISCUSSION

4.1. Interlayer Swelling. LDHs with NO_3^- or SO_4^{2-} exhibit swelling behaviors, while those with Cl^- or CO_3^{2-} do not. Swelling is dependent on the coordination structure of anions and water. The transformation from flat to tilted configurations of NO_3^- ions is responsible for the swelling. In the intermediate stage, just part of NO_3^- ions are tilted (Figure 5d), and layer puckering is responsible for the interlayer expansion. The variation of dH/dm with m, which accounts for the enthalpy change due to water immersion, is fluctuating around ca. −12 kcal/mol, without a clear trend (Figure S12 in the Supporting Information). It implies swelling is energetically available. Layer puckering needs an energy cost. And another energy cost is due to less HBs accepted by tilted NO_3^- ions and water from OH groups. However, more HBs are formed between NO_3^- ions and water (Figure 6a). Thus, the strengthening of HB interactions between water and anions compensates those energy costs to some extent. In addition, the variation of layer stacking due to polytype transition could play a role in strengthening the long-ranged Coulombic interactions. On the other hand, tilted NO_3^- ions are more flexible (Figure 5e,f,h) and so as water H-bonded to one OH group (Figure 5i). Therefore, the entropy contribution also facilitates interlayer swelling. For LDHs with CO_3^{2-}, the layer puckering is also observed at a priori high water contents, which needs an energy cost. However, although CO_3^{2-} ions exhibit similar molecular structure as NO_3^- ions, they cannot pillar layers as tilted NO_3^- ions. Thus, the puckering sets an energy barrier as shown by the high dH/dm (Figure S12 in the Supporting Information). Water and CO_3^{2-} ions in the bilayer exhibit well coordination structure (Figure 8e), implying less entropy compensation. As a result, the formation of puckering layers is not allowed at experimental humidity and thus swelling does not happen. For LDHs with Cl^-, layer puckering without anionic pillars is also observed at a priori high water contents (Figure 12b), which also explains the nonswelling behavior. For LDHs with SO_4^{2-}, dH/dm also fluctuates without a clear trend (Figure S12 in the Supporting Information), implying swelling is energetically available. The interconversion between C_{3v} and C_s configurations of SO_4^{2-} ions which pillar layers, accompanied by layer displacements with increasing water contents, facilitates swelling. In this process, the loss of HBs with layers is also largely compensated by strengthened interactions between water and SO_4^{2-} ions (Figure 6c). Certainly, the change of long-ranged Coulombic interactions due to polytype transformation could also have an influence. In summary, because of the rigidity of layers of LDHs,[106] if an anion can pillar layers through adjusting its configuration determines if an interlayer is expandable. Thus, intercalating large organic compounds[46] or exfoliation[83] is facilitated in LDHs with NO_3^- or SO_4^{2-}.

For LDHs with NO_3^-, when the Mg/Al ratio is lower, the interlayer swells at a lower water content (Figure 4a,e). Similarly, for LDHs with Cl^- or CO_3^{2-}, with a lower Mg/Al ratio the formation of a local bilayer also appears at a lower water content (Figure 4b,c,f,g). A lower Mg/Al ratio indicates a higher layer charge, so that more anions are intercalated. Thus, a lower water content is able to cause the interlayer to be crowded, leading to the formation of tilted anions or a local bilayer along with interlayer expansion. However, in the case of LDHs with SO_4^{2-}, the swelling behavior seems almost invariant with respect to Mg/Al ratio (Figure 4d,h). In this case, intercalated water splits into two layers at a lower content when the Mg/Al ratio is lower, in analogy to other cases. However, the water-bilayer formation does not accompany an adjustment of SO_4 configurations and abrupt increase in basal spacing. We deduce, with a lower Mg/Al ratio, the stronger Coulombic interactions between higher charged layers and SO_4^{2-} ions compensate the effect of "crowded water", maintaining the interlayer spacing.

4.2. Polytypism. The polytypism is correlated with the configuration of intercalated anions and the coordination relationship between anions and OH sheets. Flat NO_3^- or CO_3^{2-} ions in a monolayer, with each O atom accepting two HBs from two opposite OH groups, facilitate the P-type interlayer. The fully tilted configurations of NO_3^- ions at high water contents favor O-type interlayers. CO_3^{2-} ions cannot be transformed into tilted configurations, so that the P-type interlayer is always maintained. Similarly, for LDHs with Cl^-, water in the monolayer accepting two opposite HBs maintains the stability of a P-type interlayer. For LDHs with SO_4^{2-}, SO_4^{2-} ions with a C_s point group symmetry (Figure 10e) are more prevalent in the O-type interlayer, while the full bilayer consisting of ions and water (Figure 10i) favors the P-type interlayer.

The coordination relationship explains P- and O-type interlayers. O_1- and O_2-type interlayers make no difference in the coordination relationship between anions and OH sheets. Simply, taking only OH sheets into account, O_1- and O_2-type interlayers are symmetrical with respect to the middle plane (Figure 2e,f,h,i). However, O_1-type interlayers are less observed in our simulations. Specifically, no $3R_2$ polytype consisting of all O_1-type interlayers is found here. Only in the case of LDH-3/1-SO_4, the amount of O_1-type interlayers is comparable with that of O_2-type ones (Figure 9a). $3R_2$ polytype was also rarely reported in the literature.[58,63,69] This phenomenon cannot be explained with the coordination relationship, but it is probably due to the long-ranged energetically favorable layer stacking. It can be elucidated by the structure of brucite ($Mg(OH)_2$). Brucite is also made up of trioctahedral metal-hydroxide layers

DOI: 10.1021/acs.inorgchem.8b00949
Inorg. Chem. 2018, 57, 7299−7313

but without metal substitution (Figure 13a). The layer stacking exhibits a similar structure as the 1*T* polytype of LDHs which

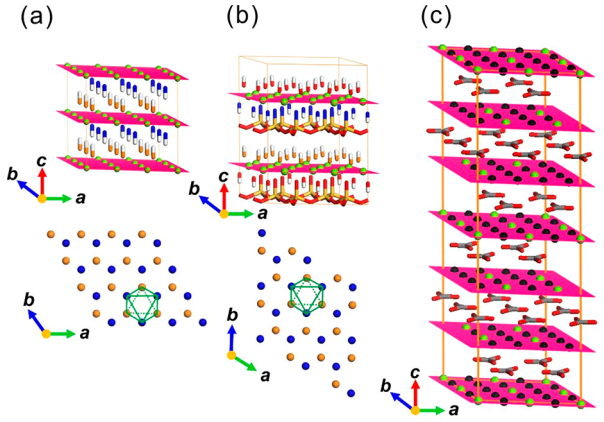

Figure 13. Schematic layer structure of brucite (a), lizardite (b), and magnesite (c). Mg, C, O, Si, and H atoms are in green, gray, red, yellow, and white, respectively. Black balls in the metallic layers of magnesite are empty sites. O atoms of the upper and lower sheets in an interlayer of brucite or lizardite are in blue and orange, respectively.

consists of all O_2-type interlayers (Figure 2c,f,i).[107,108] The O_2-type interlayer facilitates HBs between adjacent layers.[107,109] If there existed O_1-type interlayers, HBs between adjacent layers are similar. However, to our knowledge, no O_1-type interlayer has been reported for brucite. Thus, we deduce not only HBs between layers but also the long-ranged layer-stacking way determines the stability of brucite. This layer-stacking order is largely due to the long-ranged Coulombic interactions. Thence, a 1*T* polytype is favored over the $3R_2$ one for LDHs due to the similar long-ranged interactions. It is also evidenced in natural 1*T* lizardite (a layered mineral which belongs to the serpentine group and is generally associated with LDHs),[7,13,110] which has the same octahedral sheets as brucite and whose interlayer also belongs to the O_2-type (Figure 13b).[111]

The appearance of comparable amounts of O_1- and O_2-type interlayers in the case of LDH-3/1-SO_4 could be due to thermodynamics or kinetics. It is probably due to the strong HB interactions between SO_4^{2-} ions and OH sheets, which overwhelm the long-ranged Coulombic interactions. In the case of LDH-2/1-SO_4, the layered charge is higher, so that the Coulombic interactions are strengthened and almost all the interlayers are of a O_2-type. Occasional appearance of O_1-type interlayers among O_2-type ones is also observed in the case of LDHs with NO_3^- with high water contents (Figure 3a,d). In such a case, the basal spacing is large, which impairs the Coulombic interactions, favoring mixed interlayers. Certainly, the possible defect in the empirical force field, particularly the atomic charge assignment, could lead to the error estimation of the long-ranged interactions. Due to the limit of simulation time, the kinetic effect cannot be excluded. However, given that the simulated polytype transition is almost independent of initial structure (Section S2 in the Supporting Information), the kinetic effect should be minor. Nevertheless, no $3R_2$ polytype is observed here, implying such a stacking way is energetically unfavorable. The $3R_2$ polytype was suggested to be the result of cation-disordered structure,[69,112] in contrast to the cation-ordered model we simulate here. In a cation-disordered structure, Al−O−Al linkages are present,[113] and thus the local electrostatic interaction would be different.

4.3. Stability of LDHs Intercalated with Different Anions. Field and experimental studies showing mixed-metal LDHs are generally more abundant than single-metal precipitates in contaminated soil.[7−9] Allada et al. showed the heat and free energy of formation of LDHs from elements are more negative than but close to those of mechanical mixtures of binary compounds.[20−23] Specifically, they showed the free energy of $[M^{II}_{1-x}M^{III}_{x}(OH)_2](CO_3)_{x/2}\cdot mH_2O$ is just slightly lower than the sum of those of $\frac{x}{2}M^{II}CO_3$, $xM^{III}(OH)_3$, $(1-\frac{3}{2}x)M^{II}(OH)_2$, and mH_2O.[21] This is reasonable due to the structural similarity with binary compounds. In a carbonate $M^{II}CO_3$ (e.g., magnesite $MgCO_3$ in Figure 13c), CO_3 planes are also parallel to cationic layers. Moreover, if empty sites in metallic layers were filled with cations, the layer stacking of carbonate would be the same as that of LDHs of a $3R_1$ polytype. The higher stability of LDHs with CO_3^{2-} over LDHs with other anions is largely attributed to the lower solubility of $M^{II}CO_3$ in the aqueous phase.[114] Thus, the similarity with $M^{II}CO_3$ explains the stability of LDHs due to long-ranged Coulombic interactions between anions and cationic layers. On the other hand, the excess free energy of LDHs, the difference between free energies of LDHs and binary compounds, accounts for the short-ranged ionic coordination. It explains the higher stability of LDHs over binary compounds. The excess free energy follows the order $SO_4^{2-} < NO_3^- < CO_3^{2-}$.[25] It implies if only accounting for coordination structure of anions in the interlayer galleries, SO_4^{2-} ions are most stable while CO_3^{2-} ions are least. However, the formation free energies from elements exhibit a different order: $CO_3^{2-} < SO_4^{2-} < NO_3^-$,[25] consistent with the order of anion exchange capacity[24] and that of binding energy derived through previous simulations.[26] Once again, it illustrates the long-ranged Coulombic contribution plays an important role on the stability of LDHs. In addition, the stability of LDHs with CO_3^{2-} could be related to kinetics as supposed by Prasad et al.,[115] because the transition state (the swelling phase) is hard to be achieved as shown above.

However, the mechanical-mixture model does not take the transformation of polytype or anion configuration and its dependence on water content into account explicitly. It should have a major influence on the stability of LDHs and anion exchange. For example, the formation enthalpy is more negative for LDHs with CO_3^{2-} of a $3R_1$ polytype than that with intergrowth of a $2H_1$ polytype.[59] Prasanna et al. showed the anion exchange capacity is more significant in the interlayer with C_{2v} tilted NO_3^- ions than that with D_{3h} flat ones.[34] As shown in this study, C_{2v} NO_3^- ions are less hydrogen-bonded to OH sheets, so that they are more available to being exchanged. Therefore, thermodynamic studies taking water contents, anion configurations, and polytype structure into consideration, comparing results shown in this study, should be performed in the future.

5. CONCLUSIONS

MD simulations are performed to systematically disclose the dependence of polytypism of LDHs on cation ratio, anion type, and water content. LDHs intercalated with different anions (CO_3^{2-}, NO_3^-, SO_4^{2-}, and Cl^-) with Mg/Al ratios of 2/1 and 3/1 are studied with continuous water contents. For LDHs intercalated with NO_3^- ions, the polytype transition from $3R_1$ to 1*T* coincides with the transformation into fully tilted configurations of anions and a full bilayer of water in the

DOI: 10.1021/acs.inorgchem.8b00949
Inorg. Chem. 2018, 57, 7299−7313

interlayer. LDHs intercalated with CO_3^{2-} or Cl^- ions maintain a $3R_1$ polytype irrespective of water content. For LDHs intercalated with SO_4^{2-} ions, three-stage polytypism is observed with increasing water contents. When Mg/Al = 3/1, the polytype is transformed from $3R_1$ to mixed O_1- and O_2- type interlayers and then backward into $3R_1$. When Mg/Al = 2/1, it only differs in the intermediate stage when a $1T$ polytype is present. The polytype transformation coincides with the adjustment of SO_4 configurations but not well with variation of water distribution. Although SO_4^{2-} ions with a C_{3v} point group symmetry are present in different stages, the relative popularity of SO_4^{2-} ions with a C_s point group symmetry is characteristic for the intermediate polytype stage. The last $3R_1$ stage is characterized by a full bilayer consisting of anions and water. LDHs intercalated with NO_3^- or SO_4^{2-} ions exhibit swelling behaviors, because an anion can still pillar layers through adjusting its configuration while water content increases. For LDHs with NO_3^-, the swelling and polytype transition appear at a lower water content when Mg/Al is lower; while for LDHs with SO_4^{2-}, there is no such a relevance. In the cases of LDHs with CO_3^{2-} or Cl^-, the layer puckering without anionic pillars at the hypothetic high water content needs a large energy cost, which makes them nonswelling.

The configurational adjustments of anions and water reflect variations of the coordination structure, while the layer-stacking way accounts for the long-ranged Coulombic interactions. The coordination structure and long-ranged Coulombic interactions collectively determine polytypism of LDHs intercalated with different anions. The stability of LDHs in the environment is relevant to the polytype structure, which depends on cation ratio, anion type, and water content. In addition, the coordination structure influences the diffusion way of intercalated anions and water, as shown in our previous studies.[31,32] How anions are transported in the interlayer galleries is relevant to the application of LDHs as electrode or electrolyte materials.[45,116] Studying how anion movement is determined by breakage and formation of HBs should be performed in the future.

■ ASSOCIATED CONTENT

Supporting Information

The Supporting Information is available free of charge on the ACS Publications website at DOI: 10.1021/acs.inorgchem.8b00949.

Distances between hydroxyl groups in the same sheet; polytypism derived from simulations began with $1T$ polytypes; the coordination relationships between OH sheets, anions, and water; differential enthalpy as a function of water content (PDF)

■ AUTHOR INFORMATION

Corresponding Author

* E-mail: chenmeng@gig.ac.cn; Tel: +86-20-85290252; Fax: +86-20-85290252.

ORCID

Meng Chen: 0000-0002-1878-2261

Xiancai Lu: 0000-0001-8977-2661

Jianxi Zhu: 0000-0002-9002-4457

Notes

The authors declare no competing financial interest.

■ ACKNOWLEDGMENTS

This work was financially supported by Key Research Program of Frontier Sciences, Chinese Academy of Sciences (CAS) (QYZDJ-SSW-DQC023-4), and National Natural Science Foundation of China (41602034). We are grateful to the National Supercomputer Center in Guangzhou for use of the high performance computing facility. This is contribution No. IS-2541 from GIGCAS.

■ REFERENCES

(1) Drits, V.; Sokolova, T.; Sokolova, G.; Cherkashin, V. I. New members of the hydrotalcite-manasseite group. *Clays Clay Miner.* **1987**, *35*, 401−417.

(2) Crovisier, J. L.; Thomassin, J. H.; Juteau, T.; Eberhart, J. P.; Touray, J. C.; Baillif, P. Experimental seawater-basaltic glass interaction at 50°C: Study of early developed phases by electron microscopy and X-ray photoelectron spectrometry. *Geochim. Cosmochim. Acta* **1983**, *47*, 377−387.

(3) Mills, S. J.; Whitfield, P. S.; Wilson, S. A.; Woodhouse, J. N.; Dipple, G. M.; Raudsepp, M.; Francis, C. A. The crystal structure of stichtite, re-examination of barbertonite, and the nature of polytypism in MgCr hydrotalcites. *Am. Mineral.* **2011**, *96*, 179−187.

(4) Trolard, F.; Génin, J. M. R.; Abdelmoula, M.; Bourrié, G.; Humbert, B.; Herbillon, A. Identification of a green rust mineral in a reductomorphic soil by Mossbauer and Raman spectroscopies. *Geochim. Cosmochim. Acta* **1997**, *61*, 1107−1111.

(5) Juillot, F.; Morin, G.; Ildefonse, P.; Trainor, T. P.; Benedetti, M.; Galoisy, L.; Calas, G.; Brown, Jr.; Gordon, E. Occurrence of Zn/Al hydrotalcite in smelter-impacted soils from northern France: Evidence from EXAFS spectroscopy and chemical extractions. *Am. Mineral.* **2003**, *88*, 509.

(6) Nachtegaal, M.; Marcus, M. A.; Sonke, J. E.; Vangronsveld, J.; Livi, K. J. T.; van Der Lelie, D.; Sparks, D. L. Effects of in situ remediation on the speciation and bioavailability of zinc in a smelter contaminated soil. *Geochim. Cosmochim. Acta* **2005**, *69*, 4649−4664.

(7) Voegelin, A.; Pfister, S.; Scheinost, A. C.; Marcus, M. A.; Kretzschmar, R. Changes in zinc speciation in field soil after contamination with zinc oxide. *Environ. Sci. Technol.* **2005**, *39*, 6616−6623.

(8) Jacquat, O.; Voegelin, A.; Kretzschmar, R. Soil properties controlling Zn speciation and fractionation in contaminated soils. *Geochim. Cosmochim. Acta* **2009**, *73*, 5256−5272.

(9) Jacquat, O.; Voegelin, A.; Villard, A.; Marcus, M. A.; Kretzschmar, R. Formation of Zn-rich phyllosilicate, Zn-layered double hydroxide and hydrozincite in contaminated calcareous soils. *Geochim. Cosmochim. Acta* **2008**, *72*, 5037−5054.

(10) Voegelin, A.; Kretzschmar, R. Formation and dissolution of single and mixed Zn and Ni precipitates in soil: Evidence from column experiments and extended X-ray absorption fine structure spectroscopy. *Environ. Sci. Technol.* **2005**, *39*, 5311−5318.

(11) Scheidegger, A. M.; Sparks, D. L. Kinetics of the formation and the dissolution of nickel surface precipitates on pyrophyllite. *Chem. Geol.* **1996**, *132*, 157−164.

(12) Scheidegger, A. M.; Strawn, D. G.; Lamble, G. M.; Sparks, D. L. The kinetics of mixed Ni-Al hydroxide formation on clay and aluminum oxide minerals: A time-resolved XAFS study. *Geochim. Cosmochim. Acta* **1998**, *62*, 2233−2245.

(13) Scheinost, A. C.; Ford, R. G.; Sparks, D. L. The role of Al in the formation of secondary Ni precipitates on pyrophyllite, gibbsite, talc, and amorphous silica: A DRS study. *Geochim. Cosmochim. Acta* **1999**, *63*, 3193−3203.

(14) Scheinost, A. C.; Sparks, D. L. Formation of Layered Single- and Double-Metal Hydroxide Precipitates at the Mineral/Water Interface: A Multiple-Scattering XAFS Analysis. *J. Colloid Interface Sci.* **2000**, *223*, 167−178.

(15) Thompson, H. A.; Parks, G. A.; Brown, G. E. Dynamic interactions of dissolution, surface adsorption, and precipitation in an

DOI: 10.1021/acs.inorgchem.8b00949
Inorg. Chem. 2018, 57, 7299−7313

aging cobalt(II)-clay-water system. *Geochim. Cosmochim. Acta* **1999**, *63*, 1767−1779.
(16) Scheckel, K. G.; Scheinost, A. C.; Ford, R. G.; Sparks, D. L. Stability of layered Ni hydroxide surface precipitates—a dissolution kinetics study. *Geochim. Cosmochim. Acta* **2000**, *64*, 2727−2735.
(17) d'Espinose de la Caillerie, J.-B.; Kermarec, M.; Clause, O. Impregnation of γ-alumina with Ni (II) or Co (II) ions at neutral pH: Hydrotalcite-type coprecipitate formation and characterization. *J. Am. Chem. Soc.* **1995**, *117*, 11471−11481.
(18) Siebecker, M.; Li, W.; Khalid, S.; Sparks, D. Real-time QEXAFS spectroscopy measures rapid precipitate formation at the mineral−water interface. *Nat. Commun.* **2014**, *5*, DOI: 10.1038/ncomms6003.
(19) Elzinga, E. J. Formation of layered Fe(II)−Al(III)-hydroxides during reaction of Fe(II) with aluminum oxide. *Environ. Sci. Technol.* **2012**, *46*, 4894−4901.
(20) Allada, R. k.; Navrotsky, A.; Boerio-Goates, J. Thermochemistry of hydrotalcite-like phases in the MgO-Al_2O_3-CO_2-H_2O system: A determination of enthalpy, entropy, and free energy. *Am. Mineral.* **2005**, *90*, 329.
(21) Allada, R. k.; Navrotsky, A.; Berbeco, H. T.; Casey, W. H. Thermochemistry and aqueous solubilities of hydrotalcite-like solids. *Science* **2002**, *296*, 721.
(22) Allada, R. k.; Peltier, E.; Navrotsky, A.; Casey, W. H.; Johnson, C. A.; Berbeco, H. T.; Sparks, D. L. Calorimetric determination of the enthalpies of formation of hydrotalcite-like solids and their use in the geochemical modeling of metals in natural waters. *Clays Clay Miner.* **2006**, *54*, 409.
(23) Mazeina, L.; Navrotsky, A.; Dyar, D. Enthalpy of formation of sulfate green rusts. *Geochim. Cosmochim. Acta* **2008**, *72*, 1143−1153.
(24) Miyata, S. Anion-exchange properties of hydrotalcite-like compounds. *Clays Clay Miner.* **1983**, *31*, 305−311.
(25) Peltier, E.; Allada, R.; Navrotsky, A.; Sparks, D. L. Nickel solubility and precipitation in soils: A thermodynamic study. *Clays Clay Miner.* **2006**, *54*, 153−164.
(26) Li, H.; Ma, J.; Evans, D. G.; Zhou, T.; Li, F.; Duan, X. Molecular dynamics modeling of the structures and binding energies of α-nickel hydroxides and nickel− aluminum layered double hydroxides containing various interlayer guest anions. *Chem. Mater.* **2006**, *18*, 4405−4414.
(27) Wang, J.; Kalinichev, A. G.; Amonette, J. E.; Kirkpatrick, R. J. Interlayer structure and dynamics of Cl-bearing hydrotalcite: far infrared spectroscopy and molecular dynamics modeling. *Am. Mineral.* **2003**, *88*, 398−409.
(28) Kirkpatrick, R.; Kalinichev, A.; Wang, J. Molecular dynamics modelling of hydrated mineral interlayers and surfaces: structure and dynamics. *Mineral. Mag.* **2005**, *69*, 289−308.
(29) Costa, D. G.; Rocha, A. B.; Diniz, R.; Souza, W. F.; Chiaro, S. S. X.; Leitão, A. A. Structural model proposition and thermodynamic and vibrational analysis of hydrotalcite-like compounds by DFT calculations. *J. Phys. Chem. C* **2010**, *114*, 14133−14140.
(30) Frost, R. L.; Weier, M. L.; Kloprogge, J. T. Raman spectroscopy of some natural hydrotalcites with sulphate and carbonate in the interlayer. *J. Raman Spectrosc.* **2003**, *34*, 760−768.
(31) Chen, M.; Shen, W.; Lu, X.; Zhu, R.; He, H.; Zhu, J. Jumping Diffusion of Water Intercalated in Layered Double Hydroxides. *J. Phys. Chem. C* **2016**, *120*, 12924−12931.
(32) Chen, M.; Zhu, R.; Zhu, J.; He, H. Temperature-Dependent Structure and Dynamics of Water Intercalated in Layered Double Hydroxides with Different Hydration States. *J. Phys. Chem. C* **2017**, *121*, 23752−23762.
(33) Israëli, Y.; Taviot-Guého, C.; Besse, J.-P.; Morel, J.-P.; Morel-Desrosiers, N. Thermodynamics of anion exchange on a chloride-intercalated zinc−aluminum layered double hydroxide: a microcalorimetric study. *J. Chem. Soc., Dalton Trans.* **2000**, 791−796.
(34) Prasanna, S.; Kamath, P. V. Anion-Exchange Reactions of Layered Double Hydroxides: Interplay between Coulombic and H-Bonding Interactions. *Ind. Eng. Chem. Res.* **2009**, *48*, 6315−6320.
(35) Costa, D. G.; Rocha, A. B.; Souza, W. F.; Chiaro, S. S. X.; Leitão, A. A. Comparative Structural, Thermodynamic and Electronic Analyses of Zn-Al-A^{n-} Hydrotalcite-Like Compounds (A^{n-}=Cl^-, F^-, Br^-, OH^-, CO_3^{2-} or NO_3^-): An Ab Initio Study. *Appl. Clay Sci.* **2012**, *56*, 16−22.
(36) Hou, X.; Bish, D. L.; Wang, S.-L.; Johnston, C. T.; Kirkpatrick, R. J. Hydration, Expansion, Structure, and Dynamics of Layered Double Hydroxides. *Am. Mineral.* **2003**, *88*, 167−179.
(37) Lombardo, G. M.; Pappalardo, G. C.; Costantino, F.; Costantino, U.; Sisani, M. Thermal Effects on Mixed Metal (Zn/Al) Layered Double Hydroxides: Direct Modeling of the X-ray Powder Diffraction Line Shape through Molecular Dynamics Simulations. *Chem. Mater.* **2008**, *20*, 5585−5592.
(38) Rhee, S. W.; Kang, M. J. Kinetics on Dehydration Reaction during Thermal Treatment of MgAl-CO_3-LDHs. *Korean J. Chem. Eng.* **2002**, *19*, 653−657.
(39) Yu, G.; Zhou, Y.; Yang, R.; Wang, M.; Shen, L.; Li, Y.; Xue, N.; Guo, X.; Ding, W.; Peng, L. Dehydration and Dehydroxylation of Layered Double Hydroxides: New Insights from Solid-State NMR and FT-IR Studies of Deuterated Samples. *J. Phys. Chem. C* **2015**, *119*, 12325−12334.
(40) Ducos, V.; De Roy, A.; Besse, J.-P. Evolution of Protonic Conduction in [Zn−Al−Cl] Lamellar Double Hydroxide Phases with Temperature and Trivalent Metal Content. *Solid State Ionics* **2001**, *145*, 399−405.
(41) Khan, A. I.; Lei, L.; Norquist, A. J.; O'Hare, D. Intercalation and Controlled Release of Pharmaceutically Active Compounds from a Layered Double Hydroxide. *Chem. Commun.* **2001**, 2342−2343.
(42) Oh, J.-M.; Biswick, T. T.; Choy, J.-H. Layered Nanomaterials for Green Materials. *J. Mater. Chem.* **2009**, *19*, 2553−2563.
(43) Cervilla, A.; Corma, A.; Fornes, V.; Llopis, E.; Palanca, P.; Rey, F.; Ribera, A. Intercalation of $[Mo^{VI}O_2(O_2CC(S)Ph_2)_2]^{2-}$ in a Zn (II)-Al (III) Layered Double Hydroxide Host: A Strategy for the Heterogeneous Catalysis of the Air Oxidation of Thiols. *J. Am. Chem. Soc.* **1994**, *116*, 1595−1596.
(44) Li, F.; Duan, X. Applications of Layered Double Hydroxides. In *Layered Double Hydroxides*; Springer: Berlin Heidelberg, 2006; pp 193−223.
(45) Chen, H.; Hu, L.; Chen, M.; Yan, Y.; Wu, L. Nickel−Cobalt Layered Double Hydroxide Nanosheets for High-performance Supercapacitor Electrode Materials. *Adv. Funct. Mater.* **2014**, *24*, 934−942.
(46) Latterini, L.; Nocchetti, M.; Aloisi, G. G.; Costantino, U.; De Schryver, F. C.; Elisei, F. Structural, Photophysical, and Photochemical Characterization of 9-Anthracenecarboxylate−Hydrotalcite Nanocomposites: Evidence of a Reversible Light-Driven Reaction. *Langmuir* **2007**, *23*, 12337−12343.
(47) Latterini, L.; Nocchetti, M.; Aloisi, G. G.; Costantino, U.; Elisei, F. Organized chromophores in layered inorganic matrices. *Inorg. Chim. Acta* **2007**, *360*, 728−740.
(48) Gao, R.; Yan, D. Layered host-guest long-afterglow ultrathin nanosheets: high-efficiency phosphorescence energy transfer at 2D confined interface. *Chem. Sci.* **2017**, *8*, 590−599.
(49) Yan, D.; Lu, J.; Wei, M.; Li, H.; Ma, J.; Li, F.; Evans, D. G.; Duan, X. In Situ Polymerization of the 4-Vinylbenzenesulfonic Anion in Ni−Al−Layered Double Hydroxide and Its Molecular Dynamic Simulation. *J. Phys. Chem. A* **2008**, *112*, 7671−7681.
(50) Yan, D.; Lu, J.; Ma, J.; Qin, S.; Wei, M.; Evans, D. G.; Duan, X. Layered Host−Guest Materials with Reversible Piezochromic Luminescence. *Angew. Chem., Int. Ed.* **2011**, *50*, 7037−7040.
(51) Yan, D.; Lu, J.; Wei, M.; Ma, J.; Evans, D. G.; Duan, X. A combined study based on experiment and molecular dynamics: perylene tetracarboxylate intercalated in a layered double hydroxide matrix. *Phys. Chem. Chem. Phys.* **2009**, *11*, 9200−9209.
(52) Yan, D.; Lu, J.; Ma, J.; Wei, M.; Qin, S.; Chen, L.; Evans, D. G.; Duan, X. Thin film of coumarin-3-carboxylate and surfactant co-intercalated layered double hydroxide with polarized photoluminescence: a joint experimental and molecular dynamics study. *J. Mater. Chem.* **2010**, *20*, 5016−5024.
(53) Arrhenius, G.; Sales, B.; Mojzsis, S.; Lee, T. Entropy and Charge in Molecular Evolution—the Case of Phosphate. *J. Theor. Biol.* **1997**, *187*, 503−522.

DOI: 10.1021/acs.inorgchem.8b00949
Inorg. Chem. 2018, 57, 7299−7313

(54) Arrhenius, G. O. Crystals and life. *Helv. Chim. Acta* **2003**, *86*, 1569−1586.
(55) Jobbágy, M. a.; Iyi, N. Interplay of charge density and relative humidity on the structure of nitrate layered double hydroxides. *J. Phys. Chem. C* **2010**, *114*, 18153−18158.
(56) Thyveetil, M.-A.; Coveney, P. V.; Suter, J. L.; Greenwell, H. C. Emergence of undulations and determination of materials properties in large-scale molecular dynamics simulation of layered double hydroxides. *Chem. Mater.* **2007**, *19*, 5510−5523.
(57) Bookin, A.; Drits, V. Polytype diversity of the hydrotalcite-like minerals. I. Possible polytypes and their diffraction features. *Clays Clay Miner.* **1993**, *41*, 551−557.
(58) Bookin, A.; Cherkashin, V.; Drits, V. Polytype diversity of the hydrotalcite-like minerals; II, Determination of the polytypes of experimentally studied varieties. *Clays Clay Miner.* **1993**, *41*, 558−564.
(59) Shivaramaiah, R.; Navrotsky, A. Energetics of order−disorder in layered magnesium aluminum double hydroxides with interlayer carbonate. *Inorg. Chem.* **2015**, *54*, 3253−3259.
(60) Britto, S.; Kamath, P. V. Polytypism, disorder, and anion exchange properties of divalent ion (Zn, Co) containing bayerite-derived layered double hydroxides. *Inorg. Chem.* **2010**, *49*, 11370−11377.
(61) Britto, S.; Kamath, P. V. Polytypism in the Lithium−Aluminum Layered Double Hydroxides: The $[LiAl_2(OH)_6]^+$ Layer as a Structural Synthon. *Inorg. Chem.* **2011**, *50*, 5619−5627.
(62) Roudebush, J. H.; Sahasrabudhe, G.; Bergman, S. L.; Cava, R. Rhombohedral Polytypes of the Layered Honeycomb Delafossites with Optical Brilliance in the Visible. *Inorg. Chem.* **2015**, *54*, 3203−3210.
(63) Mills, S.; Christy, A.; Génin, J.-M.; Kameda, T.; Colombo, F. Nomenclature of the hydrotalcite supergroup: natural layered double hydroxides. *Mineral. Mag.* **2012**, *76*, 1289−1336.
(64) Taylor, H. Crystal structures of some double hydroxide minerals. *Mineral. Mag.* **1973**, *39*, 377−389.
(65) Pausch, I.; Lohse, H.-H.; Allmann, R. Syntheses of disordered and A1-rich hydrotalcite-like compounds. *Clays Clay Miner.* **1986**, *34*, 507−510.
(66) Ingram, L.; Taylor, H. The crystal structures of sjogrenite and pyroaurite. *Mineral. Mag. J. Mineral. Soc.* **1967**, *36*, 465−479.
(67) Grguric, B.; Madsen, I.; Pring, A. Woodallite, a new chromium analogue of iowaite from the Mount Keith nickel deposit, Western Australia. *Mineral. Mag.* **2001**, *65*, 427−435.
(68) Braithwaite, R.; Dunn, P.; Pritchard, R.; Parr, W. Iowaite, a reinvestigation. *Mineral. Mag.* **1994**, *58*, 79−85.
(69) Radha, S.; Kamath, P. V. Polytypism in sulfate-intercalated layered double hydroxides of Zn and M (III)(M= Al, Cr): Observation of cation ordering in the metal hydroxide layers. *Inorg. Chem.* **2013**, *52*, 4834−4841.
(70) Witzke, T.; Raade, G. Zincowoodwardite, $[Zn_{1-x}Al_x(OH)_2]$-$[(SO_4)_{x/2}(H_2O)_n]$, a new mineral of the hydrotalcite group. *N. Jb. Miner. Mh.* **2000**, *10*, 455−465.
(71) Bish, D. L. Anion-exchange in takovite: applications to other hydroxide minerals. *Bull. Mineral.* **1980**, *103*, 5.
(72) Nickel, E. H.; Wildman, J. E. Hydrohonessite−a new hydrated Ni-Fe hydroxysulphate mineral; its relationship to honessite, carrboydite and minerals of the pyroaurite group. *Mineral. Mag.* **1981**, *44*, 333−337.
(73) Bellotto, M.; Rebours, B.; Clause, O.; Lynch, J.; Bazin, D.; Elkaïm, E. A reexamination of hydrotalcite crystal chemistry. *J. Phys. Chem.* **1996**, *100*, 8527−8534.
(74) Evans, D. G.; Slade, R. C. Structural aspects of layered double hydroxides. In *Layered double hydroxides*; Springer: Berlin Heidelberg, 2006; pp 1−87.
(75) Marappa, S.; Radha, S.; Kamath, P. V. Nitrate-Intercalated Layered Double Hydroxides−Structure Model, Order, and Disorder. *Eur. J. Inorg. Chem.* **2013**, *2013*, 2122−2128.
(76) Xu, Z.; Zeng, H. Abrupt Structural Transformation in Hydrotalcite-like Compounds $Mg_{1-x}Al_x(OH)_2(NO_3)_xnH_2O$ as a Continuous Function of Nitrate Anions. *J. Phys. Chem. B* **2001**, *105*, 1743−1749.
(77) Wang, S.-L.; Wang, P.-C. In situ XRD and ATR-FTIR study on the molecular orientation of interlayer nitrate in Mg/Al-layered double hydroxides in water. *Colloids Surf., A* **2007**, *292*, 131−138.
(78) Sjåstad, A. O.; Andersen, N. H.; Vajeeston, P.; Karthikeyan, J.; Arstad, B.; Karlsson, A.; Fjellvåg, H. On the Thermal Stability and Structures of Layered Double Hydroxides $Mg_{1-x}Al_x(OH)_2(NO_3)_x$·$mH_2O$ ($0.18 \leqslant x \leqslant 0.38$). *Eur. J. Inorg. Chem.* **2015**, *2015*, 1775−1788.
(79) Brunger, A. T.; Krukowski, A.; Erickson, J. W. Slow-Cooling Protocols for Crystallographic Refinement by Simulated Annealing. *Acta Crystallogr., Sect. A: Found. Crystallogr.* **1990**, *46*, 585−593.
(80) Costa, D. G.; Rocha, A. B.; Souza, W. F.; Chiaro, S. S. X.; Leitão, A. A. Ab Initio Simulation of Changes in Geometry, Electronic Structure, and Gibbs Free Energy Caused by Dehydration of Hydrotalcites Containing Cl^- and CO_3^{2-} Counteranions. *J. Phys. Chem. B* **2011**, *115*, 3531−3537.
(81) Yan, H.; Wei, M.; Ma, J.; Evans, D. G.; Duan, X. Plane-wave density functional theory study on the structural and energetic properties of cation-disordered Mg− Al layered double hydroxides. *J. Phys. Chem. A* **2010**, *114*, 7369−7376.
(82) Hou, X.; Kalinichev, A. G.; Kirkpatrick, R. J. Interlayer Structure and Dynamics of Cl^-− $LiAl_2$-Layered Double Hydroxide: ^{35}Cl NMR Observations and Molecular Dynamics Modeling. *Chem. Mater.* **2002**, *14*, 2078−2085.
(83) Song, F.; Hu, X. Exfoliation of layered double hydroxides for enhanced oxygen evolution catalysis. *Nat. Commun.* **2014**, *5*, 4477.
(84) Sideris, P. J.; Nielsen, U. G.; Gan, Z.; Grey, C. P. Mg/Al ordering in layered double hydroxides revealed by multinuclear NMR spectroscopy. *Science* **2008**, *321*, 113−117.
(85) Richardson, I. G. Clarification of possible ordered distributions of trivalent cations in layered double hydroxides and an explanation for the observed variation in the lower solid-solution limit. *Acta Crystallogr., Sect. B: Struct. Sci., Cryst. Eng. Mater.* **2013**, *69*, 629−633.
(86) Plimpton, S. Fast Parallel Algorithms for Short-Range Molecular Dynamics. *J. Comput. Phys.* **1995**, *117*, 1−19.
(87) Cygan, R. T.; Liang, J.-J.; Kalinichev, A. G. Molecular Models of Hydroxide, Oxyhydroxide, and Clay Phases and the Development of a General Force Field. *J. Phys. Chem. B* **2004**, *108*, 1255−1266.
(88) Berendsen, H. J.; Postma, J. P.; van Gunsteren, W. F.; Hermans, J. Interaction Models for Water in Relation to Protein Hydration. In *Intermolecular forces*; Springer: Dordrecht, 1981; pp 331−342.
(89) Wang, J.; Kalinichev, A. G.; Kirkpatrick, R. J. Effects of Substrate Structure and Composition on the Structure, Dynamics, and Energetics of Water at Mineral Surfaces: A Molecular Dynamics Modeling Study. *Geochim. Cosmochim. Acta* **2006**, *70*, 562−582.
(90) Wang, J.; Becker, U. Structure and carbonate orientation of vaterite ($CaCO_3$). *Am. Mineral.* **2009**, *94*, 380.
(91) Baaden, M.; Burgard, M.; Wipff, G. TBP at the Water−Oil Interface: The Effect of TBP Concentration and Water Acidity Investigated by Molecular Dynamics Simulations. *J. Phys. Chem. B* **2001**, *105*, 11131−11141.
(92) Williams, C. D.; Burton, N. A.; Travis, K. P.; Harding, J. H. The Development of a Classical Force Field To Determine the Selectivity of an Aqueous Fe^{3+}−EDA Complex for TcO_4^- and SO_4^{2-}. *J. Chem. Theory Comput.* **2014**, *10*, 3345−3353.
(93) Hockney, R. W.; Eastwood, J. W. *Computer Simulation Using Particles*; CRC Press: New York, 1988.
(94) Berendsen, H. J. C.; Postma, J. P. M.; van Gunsteren, W. F.; DiNola, A.; Haak, J. R. Molecular dynamics with coupling to an external bath. *J. Chem. Phys.* **1984**, *81*, 3684−3690.
(95) Nosé, S.; Klein, M. Constant Pressure Molecular Dynamics for Molecular Systems. *Mol. Phys.* **1983**, *50*, 1055−1076.
(96) Parrinello, M.; Rahman, A. Polymorphic Transitions in Single Crystals: A New Molecular Dynamics Method. *J. Appl. Phys.* **1981**, *52*, 7182−7190.
(97) Hoover, W. G. Canonical Dynamics: Equilibrium Phase-Space Distributions. *Phys. Rev. A: At., Mol., Opt. Phys.* **1985**, *31*, 1695.

DOI: 10.1021/acs.inorgchem.8b00949
Inorg. Chem. 2018, 57, 7299−7313

(98) Nosé, S. A Molecular Dynamics Method for Simulations in the Canonical Ensemble. *Mol. Phys.* **1984**, *52*, 255−268.
(99) Lingenheil, M.; Denschlag, R.; Reichold, R.; Tavan, P. The "Hot-Solvent/Cold-Solute" Problem Revisited. *J. Chem. Theory Comput.* **2008**, *4*, 1293−1306.
(100) Parthasarathy, G.; Lakshmi Kantam, M.; Choudary, B. M.; Venkat Reddy, C. Pressure-induced phase transitions of hydrotalcite by electrical resistivity, structural and thermal studies. *Microporous Mesoporous Mater.* **2002**, *56*, 147−152.
(101) Jayanthi, K.; Nagendran, S.; Kamath, P. V. Layered double hydroxides: proposal of a one-layer cation-ordered structure model of monoclinic symmetry. *Inorg. Chem.* **2015**, *54*, 8388−8395.
(102) Iyi, N.; Fujii, K.; Okamoto, K.; Sasaki, T. Factors influencing the hydration of layered double hydroxides (LDHs) and the appearance of an intermediate second staging phase. *Appl. Clay Sci.* **2007**, *35*, 218−227.
(103) Jayanthi, K.; Kamath, P. V. A Crystal Chemical Approach to a Cation-Ordered Structure Model for Carbonate-Intercalated Layered Double Hydroxides. *Cryst. Growth Des.* **2016**, *16*, 4450−4456.
(104) Cavani, F.; Trifirò, F.; Vaccari, A. Hydrotalcite-type anionic clays: Preparation, properties and applications. *Catal. Today* **1991**, *11*, 173−301.
(105) Radha, S.; Jayanthi, K.; Breu, J.; Kamath, P. V. Relative Humidity-Induced Reversible Hydration Of Sulfate-Intercalated Layered Double Hydroxides. *Clays Clay Miner.* **2014**, *62*, 53−61.
(106) Hines, D. R.; Solin, S. A.; Costantino, U.; Nocchetti, M. Physical properties of fixed-charge layer double hydroxides. *Phys. Rev. B: Condens. Matter Mater. Phys.* **2000**, *61*, 11348−11358.
(107) Parise, J. B. Pressure-induced H bonding: Neutron diffraction study of brucite, $Mg(OD)_2$, to 9.3 GPa. *Am. Mineral.* **1994**, *79*, 193−196.
(108) Nagai, T.; Hattori, T.; Yamanaka, T. Compression mechanism of brucite: An investigation by structural refinement under pressure. *Am. Mineral.* **2000**, *85*, 760−764.
(109) Mookherjee, M.; Stixrude, L. High-pressure proton disorder in brucite. *Am. Mineral.* **2006**, *91*, 127−134.
(110) Hudson, D.; Bussell, M. Mountkeithite, a new pyroaurite-related mineral with an expanded interlayer containing exchangeable $MgSO_4$. *Mineral. Mag.* **1981**, *44*, 345−350.
(111) Mellini, M. The crystal structure of lizardite 1T; hydrogen bonds and polytypism. *Am. Mineral.* **1982**, *67*, 587−598.
(112) Jayanthi, K.; Kamath, P. V. Observation of cation ordering and anion-mediated structure selection among the layered double hydroxides of Cu (II) and Cr (III). *Dalton Trans.* **2013**, *42*, 13220−13230.
(113) Cadars, S.; Layrac, G.; Gérardin, C.; Deschamps, M.; Yates, J. R.; Tichit, D.; Massiot, D. Identification and Quantification of Defects in the Cation Ordering in Mg/Al Layered Double Hydroxides. *Chem. Mater.* **2011**, *23*, 2821−2831.
(114) Allada, R. K.; Pless, J. D.; Nenoff, T. M.; Navrotsky, A. Thermochemistry of hydrotalcite-like phases intercalated with CO_3^{2-}, NO_3^-, Cl^-, I^-, and ReO_4. *Chem. Mater.* **2005**, *17*, 2455−2459.
(115) Prasad, B. E.; Kamath, P. V.; Vijayamohanan, K. Anion exchange reaction potentials as approximate estimates of the relative thermodynamic stabilities of Mg/Al layered double hydroxides containing different anions. *Langmuir* **2011**, *27*, 13539−13543.
(116) Kim, H.-S.; Yamazaki, Y.; Kim, J.-D.; Kudo, T.; Honma, I. High ionic conductivity of Mg−Al layered double hydroxides at intermediate temperature (100−200°C) under saturated humidity condition (100% RH). *Solid State Ionics* **2010**, *181*, 883−888.

DOI: 10.1021/acs.inorgchem.8b00949
Inorg. Chem. 2018, 57, 7299−7313